BNL-104753-2014-TECH

AGS/AD/Tech Note No. 337;BNL-104753-2014-IR

BEAM LOSS AND INDUCED ACTIVATION IN THE AGS

K. A. Brown

April 1990

Collider Accelerator Department

Brookhaven National Laboratory

U.S. Department of Energy

USDOE Office of Science (SC)

DISCLAIMER

Accelerator Division
Alternating Gradient Synchrotron Department
BROOKHAVEN NATIONAL LABORATORY
Upton, New York 11973

Accelerator Division
Technical Note

AGS/AD/Tech. Note No. 337

BEAM LOSS AND INDUCED ACTIVATION IN THE AGS

Kevin Brown

April 9, 1990

TABLE OF CONTENTS

I. INTRODUCTION

In previous notes[1-5], activation and beam loss data have been presented for various operating conditions at the AGS. In this note, activation and beam loss will be studied in more detail. This study will make use of data from residual activation measurements, beam loss as measured from intensity monitors, and beam loss as seen on ionization chambers. The operating conditions will be two slow extracted beam runs (SEB runs in January 1987 and April 1988) in which there was high intensity protons (up to 1.4×10^{13} ppp extracted beam). Data were taken during the 1989 SEB run (in which were ran 1.6×10^{13} ppp) but a large amount of the data still has not been analyzed. Also, the reliability of the RLRM system was unusually bad, causing a lot of the data to be questionable. The system is getting old and desperately needs the upgrades presently being designed.

The objective of this experiment is to determine the constants of proportionality which would allow direct comparison of instantaneous beam losses to the resulting activation around the AGS. The determination of these constants will lead to better predictions of future activation as well as further our understanding of the AGS RLRM monitor system. Two sets of constants are considered of interest. The first is the values of k in the Sullivan - Overton relationship (derived in Section II) versus the energy of beam at the time of a particular loss. The next set of constants are the factors needed to normalize out geometrical differences in the AGS ring (which is called g). Once these constants are known, the prediction of activation will be straight forward.

According to Sullivan and Overton[6,7], the dose rate from radioactivity induced by high energy particles interacting with a material such that a large number of isotopes are produced can be expressed by

$$D = k \cdot \xi \cdot \ln (1 + T/t)$$

where ξ is the number of high energy particles per interaction and k is a constant for any set of irradiation, target, and geometrical conditions. The time T is the amount of time the material was bombarded with high energy particles (the irradiation time) and the time t is the time elapsed after the bombardment stopped (the cooldown time). There are two basic assumptions behind this relationship. The first is that a sufficiently large number of different isotopes are produced by spallation reactions such that the "half-life distribution" among isotopes can be approximated by a continuous function. The second is since activity is not measured until after some 15 minutes of cooldown has lapsed and before a period of two years has elapsed, reasonable limits can be placed on this continuous

function to enable a relatively simple expression to be derived.

To obtain values of k, measurements of D are taken from a number of Health Physics AGS surveys and measurements of ξ are taken regularly during a run of length T. Section III discusses how the health physics data is used to derive the portion of the activation due to the beam losses in a run of length T. From surveys taken before a run, an estimated background activation is found. From this and a survey taken after a run, an estimate of the activation due to beam loss during that run is made. Figures 4 and 5 show the added activations for the two runs. Beam losses are obtained from ionization monitors distributed around the AGS along with changes in the beam current as measured by various beam current monitors. Measurements of these losses are taken regularly during the run. Figures 6 - 11 show the beam loss distributions for the two runs. Table I (p. 13) gives the amounts of beam loss for the two runs. Section IV discusses how these data are taken and summarized to enable a single set of data to be used for comparison to the activation data. Section V discusses how these two sets of data are compared to obtain values of k and g (the geometrical factors).

In Section II, an approximate value for k is calculated. This value does not take into account the complex geometry of the AGS, and serves only as a reference to understand the approximate order of magnitude of the experimentally determined constants. In particular it does not consider the effects of secondary emissions due to cascades in high energy beam losses in thick targets. The calculated value is

$$k = 5.3 \times 10^{-14} \text{ mR/proton.}$$

Note that the units are given as mR/proton. Arguably, the units are actually mR/hr/proton/hr. The hours were cancelled for convenience.

Figure 18 shows the experimentally found values versus the beam energy. It is interesting to note that values of k found in previous studies (old values) fall very closely to these newly determined values (new values). The old values are included in Fig. 18 for reference. The method for the determination of the old values was different from that used here and so they were expected to be different. That the old values are consistently greater than the new ones is probably due to the extraction of the geometrical factors g from the new constants. Figures 12 through 16 show the values of k/g versus the position in a superperiod. There is seen a very dramatic difference between the upstream (US) and downstream (DS) halves of a superperiod.

Tables III and IV (pp. 19 and 21) summarize the values of the k's and g's. In Appendix II the values of k/g are found with least square fits and the chi-squares are determined.

Section VI summarizes the methods used at CERN in their studies of beam loss and activation. Values of k are derived from their data to enable comparisons to this work. Table VII (p. 25) summarizes all the values of k.

II. SULLIVAN - OVERTON RELATIONSHIP

1. Derivation

(Much of what is contained in this section can be found treated in Refs. 8 and 10).

It is assumed that a sufficiently large number of different isotopes are produced by spallation reactions such that the "half-life distribution" among isotopes can be approximated by a continuous function.

The number of radioactive nuclei of ν produced per unit volume per unit time is:

$$N_\nu = \Phi \cdot N_T \cdot \sigma_{T,\nu}$$

where N_T = number of target atoms per unit volume
Φ = flux of incident particles (number particles/cm^2 sec)
$\sigma_{T,\nu}$ = cross section leading from target nucleus (τ) to desired isotope (ν).

For a target of density ρ

$n_\nu = N_{\nu/\rho}$ = number of nuclei of ν/gm of target material
$n_\tau = N_{T/\rho}$ = number of target atoms/gm of target material.

{recall → $N_0 = 6.02 \times 10^{23}$ atoms/mole.}

For a target material of atomic weight A_T, the number of nuclei of isotope ν per gram of target material produced per unit time is

$$n_\nu = \Phi \cdot \frac{N_0}{A_T} \cdot \sigma_{T,\nu}.$$

Define the mean-life and half-life of isotope ν as, respectively, t_ν and $t_{1/2,\nu}$. Then

$$t_\nu = \frac{1}{\ln 2} \cdot t_{1/2,\nu}$$

The law of decay states that

$$n_\nu(t) = n_\nu(0) \exp(-t/t_\nu).$$

If t_i is the time for which the material was irradiated then

$$n_\nu(t_i) = \Phi \cdot \frac{N_0}{A_T} \cdot \sigma_{T,\nu} \int_0^{t_i} \exp\left\{-\frac{(t_i - \tau)}{t_\nu}\right\} d\tau$$

then

$$n_\nu(t_i) = \Phi \cdot \frac{N_0}{A_T} \cdot \sigma_{T,\nu} \cdot t_\nu \cdot [1 - \exp\{-t_i/t_\nu\}]$$

If t_c is the time to elapse without further irradiation, the "cooling" time, then the number of nuclei of isotope ν would decrease to

$$n_\nu(t_i, t_c) = \Phi \cdot \frac{N_0}{A_T} \sigma_{T,\nu} \cdot t_\nu \cdot [1 - \exp\{-t_i/t_\nu\}] \cdot \exp(-t_c/t_\nu)$$

This is the activation formula for one particular isotope.

The total activity of the target is the sum of all the disintegration rates of all the different isotopes:

$\therefore$

$$a = -\sum_\nu \frac{dn_\nu}{dt_c} = \Phi \cdot \frac{N_0}{A_T} \cdot \sum_\nu \sigma_{T,\nu} \cdot [1 - \exp\{-t_i/t_\nu\}] \cdot \exp(-t_c/t_\nu)$$

(which is disintegrations /sec/gm).

This can be rewritten as

$$a = \text{const.} \int_{t_{\nu 1}}^{t_{\nu 2}} \{1 - \exp(-t_i/t_\nu)\} \cdot \exp(-t_c/t_\nu) dN(t_\nu)$$

where we are now concerned only with the activation due to those isotopes with mean lives between $t_{\nu 1}$ and $t_{\nu 2}$.

Substitute $dN(t_\nu) = \frac{b}{t_\nu} dt_\nu$

and $\lambda = 1/t_\nu \quad (d\lambda = -\frac{1}{t_\nu{}^2} \cdot dt_\nu)$

then

$$a = \text{const.} \cdot b \int_{\lambda_2}^{\lambda_1} \left\{ \exp.(-\lambda t_c) - \exp.\{-\lambda (t_i + t_c)\} \right\} \frac{1}{\lambda} \, d\lambda$$

This integral is of the type

$$\int_{\chi}^{\infty} \frac{e^{-u}}{u} \, du = - \text{Ei}\ (-\chi), \quad o < \chi < \infty$$

which is the {first, $E_1(\chi)$} exponential integral function. This expands to, for $\chi \to 0$ (see Appendix III),

$$\text{Ei}(-\chi) = \gamma + \ln x + \sum_{n=1}^{\infty} (-1)^n \frac{\chi^n}{n \cdot n!}$$

(γ = Euler - Mascheroni constant = 0.5772).

So;

$$a = \text{Const. } b \cdot \left\{ \text{Ei}\ (-\lambda_1 \cdot t_c) - \text{Ei}\ (-\lambda_2 \cdot t_c) - \text{Ei}\ [-\lambda_1 \cdot (t_c + t_i)] + \right.$$

$$\left. \text{Ei}\ [-\lambda_2\ (t_c + t_i)] \right\}.$$

For values up to $\chi = 2$, a limit can be set beyond which the function $\text{Ei}(-\chi)$ is practically zero.

For $\lambda_1 \cdot t_c > 2$ & $\lambda_1 \cdot (t_c + t_i) > 2$

$$t_c > \frac{2}{\lambda_1} \quad \text{or} \simeq \ 12 \text{ minutes.}$$

For values of χ which are small with respect to 1 ($\chi \leq 1/3$)

$$- \text{Ei}(-\chi) = - c - \ln \chi$$

the upper limit is $t_c + t_i < 1/3\ \lambda_2$ or $\simeq 5 \times 10^2$ days.
It is therefore easy to see that

$$a = \text{Const.} \cdot b \cdot \ln \left\{ \frac{t_i + t_c}{t_c} \right\} .$$

2. A Relationship for the Constant k

From the above relationship for a, we see that

$$\text{Const. } b = \Phi \cdot \frac{N_o}{A_T} \cdot \sum_{\nu} \sigma_{T,\nu} \cdot \frac{1}{t\nu} \cdot \frac{dN\ (t_\nu)}{dt_\nu} .$$

From the Sullivan - Overton relationship, then

$$k \cdot \xi \propto \Phi \cdot \frac{N_o}{A_T} \cdot \sum_{\nu} \sigma_{T,\nu} \cdot \frac{1}{t\nu} \cdot \frac{dN\ (t_\nu)}{dt_\nu} .$$

From the definition of Φ we have

$$\frac{\Phi}{\xi} = \frac{\xi}{\alpha} \cdot \frac{1}{\xi}$$

where α is the cross-sectional area of interaction (of beam on target material). Then,

$$k \propto \frac{1}{\alpha} \cdot \frac{N_o}{A_T} \sum_{\nu} \sigma_{T,\nu} \cdot \frac{1}{t\nu} \cdot \frac{dN\ (t_\nu)}{dt_\nu} .$$

Defining $n(\lambda)d\lambda$ as the number of isotopes in the decay constant range from λ to $\lambda + d\lambda$, then

$$\sum_{\nu} \sigma_{T,\nu} \cdot \frac{1}{t_\nu} \cdot \frac{dN\ (t_\nu)}{dt_\nu} = \bar{\sigma}_s \int_{\lambda_1}^{\lambda_2} n\ (\lambda)\ d\lambda$$

where $\bar{\sigma}_s$ is the average isotopic production cross-section. If we assume that the fraction of isotopes produced that have decay constant between λ_2 and λ_1 is a constant, then (calling the fraction f);

$$\bar{\sigma}_s \int_{\lambda_1}^{\lambda_2} n(\lambda)\, d\lambda = f\, \sigma_{tot.}$$

so;

$$k \propto \frac{1}{\alpha} \frac{N_o}{A_T} \cdot f\, \sigma_{tot.}$$

$$D \propto \frac{S \cdot E \cdot \mu}{4\pi\, r^2} \quad \text{(Ref. \#6)}$$

where S is the gamma activity, E is the energy of absorbed gammas (average), μ is the mass energy absorption coefficient, and r is the distance from the source. If we consider that E, μ, and r are constants, then

$$k = \frac{C}{\alpha} \cdot \frac{N_o}{A_T} \cdot f \cdot \sigma_{tot.} \quad \text{dis/gm.}$$

The conversion from dis/gm to rad is 6.24×10^7 (MeV/gm). Since the measured radiation is gammas, the Q is 1, and so;

$$k = \frac{C}{6.24 \times 10^7} \cdot \frac{1}{\alpha} \cdot \frac{N_o}{A_T} \cdot f \cdot \sigma_{tot.} \quad \text{rem/proton.}$$

where $C = \frac{E \cdot \mu}{4\pi r^2}$

3. Calculation of k

To see what order of magnitude to expect of k take;

$E = 1$ MeV (average energy of absorbed gammas)
$\mu = 0.032$ (cm^2/gm)
$r = 30.5$ cm
$A_T = 64$
$\alpha = \pi cm^2$
$f = 0.5$

and $\sigma_{tot.} = 800$ mb (1 barn = 10^{-24} cm^2)

(Note: $\sigma_{tot.} = 15.9\ \pi\ A^{2/3}$ from Sullivan[6])

we then get

$k = 5.3 \times 10^{-17}$ rem/proton ($= 5.3 \times 10^{-14}$ mR/proton)

Note that the energy of the incident particles is not directly considered. We should expect, because of the increasingly large number of secondary interactions caused by higher energy particles (cascades due to thick targets) that k is a function of the energy of the incident particles also. The cross-section is defined for interactions in which the energy loss of the particles is negligible. The typical interaction in the AGS is in targets which are thick with respect to an interaction (radiation length) length, yet not thick (or not always) with respect to a range length. It is therefore difficult to quantify the constant k beyond the above definition without getting into details of geometry and beam loss mechanisms. A treatment of this type is beyond the scope of this report.

III. RESIDUAL ACTIVATION

1. Health Physics AGS Ring Surveys

Health Physics technicians perform a recorded ring survey and take 478 measurements of residual activation. Each measurement is made using a fixed geometry probe at 12 inches. The survey point is made at the downstream end of every main magnet. In the 5 foot straight sections the highest reading is recorded. Two hundred and thirty eight measurements are made on the outside of the ring and 240 measurements are made on the inside of the ring. A single measurement is made approximately every 1.50° of the machine radius. Prior to 1989, the typical instrument used in these surveys was the West German Automess Teletector 6112B.

Since RLRM monitors subtend 3° of the machine radius on the outside of the ring, how one treats the H.P. data greatly effects any comparison between the two. In this report, the maximum H.P. measurement (outer) was taken every 3° (corresponding to the same 3° subtended by the RLRM monitors).

Figures 1 and 2 show the H.P. surveys for the two runs.

2. Estimation of Background Activation

Since the activation measured at some time t is due to beam losses over the lifetime of the AGS, the dose due to the most recent activation must be subtracted out in order to compare the induced activation to the ionization chamber and beam loss data.

Suppose there are two H.P. surveys, h_1 and h_2, between which there has been no added activation, and therefore should measure the background cooling rate (assume the two sets of measurements are taken a reasonably long time after the last activation so that only long lived isotopes are considered). From these two surveys, we can write two equations (for each location in the sets of measurements). These two equations have two unknowns, which are called T_{eff} and $k\xi_{eff}$. These two unknowns represent the activation history of the AGS.

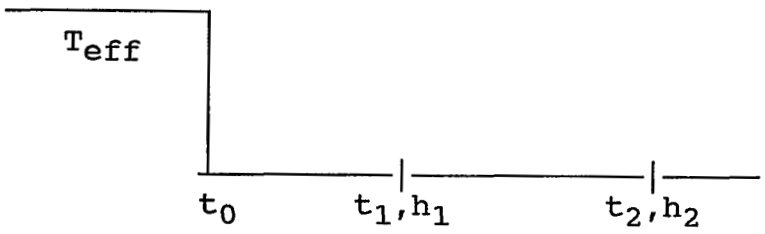

from Sullivan[6];

$$D = k \cdot \xi \cdot \ln (1 + T/t)$$

so, $$h_1 = k \cdot \xi_{eff} \cdot \ln (1 + T_{eff}/\{t_1 - t_0\})$$

$$h_2 = k \cdot \xi_{eff} \cdot \ln (1 + T_{eff}/\{t_2 - t_0\})$$

then,

$$\frac{h_1}{\ln\,(1 + T_{eff}/\{t_1 - t_0\})} = \frac{h_2}{\ln\,(1 + T_{eff}/\{t_2 - t_0\})}$$

or

$$T_{eff} = \frac{(t_1 - t_0) \cdot (t_2 - t_0)}{(t_2 - t_1)} \cdot e^{h_1/h_2}$$

$$k \cdot \xi_{eff} = \frac{h_2}{\ln\,(1 + T_{eff}/\{t_2 - t_0\})}$$

Now suppose that after h_2 there is a run which adds to the activation.

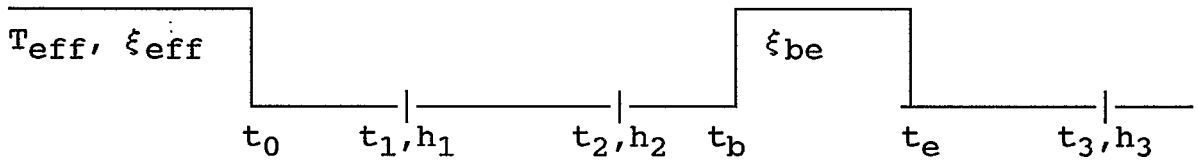

We now know T_{eff} and ξ_{eff}. Therefore, suppose at t_3 there was no added activation, then,

$$h_3' = k \cdot \xi_{eff} \cdot \ln\,\{1 + T_{eff}/(t_3 - t_0)\}$$

is the background activation at time t_3.

Figure 3 shows the background activations estimated from surveys taken in July 1986 and December 1986 for the January 1987 run.

2. Estimation of Activation Due to the Most Recent Beam Loss

We must now assume that the activation contribution from the most recent activation and the background activation are simply additive.

$$h_3 - h_3' \equiv h_{act}$$

and

$$h_{act} \equiv k \cdot \xi_{be} \cdot \ln\left(1 + \frac{t_e - t_b}{t_3 - t_e}\right)$$

where ξ_{be} is the average beam loss (p/hr) between t_e and t_b.

In the data analyzed in this report, the first run (January 1987) had enough data that it could be treated with this analysis. For the second run (April 1988) this was not the case. In this case there happened to be two runs after the pair of background measurements. Because there was an H.P. survey between the two runs, though, it made it possible to calculate the background and the added activation simply using the same method as outlined above.

Figures 4 and 5 show the added activations for the two runs.

IV. BEAM LOSS MEASUREMENTS

1. RLRM Data

There are 120 ionization chamber monitors distributed around the AGS ring, one every 3°. Each monitor is located on the underside of the main magnet girders along the outside of the ring. These subtend two main magnets, the upstream being an odd numbered magnet (i.e., the A10 monitor subtends magnets A9 and A10). A program on the PDP10, called RLRM, is used to sample these monitors at different times in the AGS cycle (only one time slice can be made at a time). A batch file was written which ran the RLRM program for three different time slices (corresponding to injection, transition, and extraction) every 12 hours for the length of the runs. At the end of a run, a total of N measurements had been made of beam loss distributions around the ring. A single measurement is called $r(\phi,\epsilon,n)$, where ϕ is the position (every 3°), ϵ corresponds to the energy, and n represents one of N samples. Since the effect of a beam loss ξ_n decreases at some rate R_n, where ξ_n corresponds to a measurement made at a time t_n, then the weighted average beam loss distribution at the end of the run will be;

$$\langle r\ (\phi,\epsilon)\rangle = \frac{\sum_n r(\phi,\epsilon,n)\cdot R_n}{\sum_n R_n}\ .$$

If we take R_n as

$$R_n = \ln\ (1 + \frac{t_w}{t_f - t_n}\ ),$$

where t_w is the amount of time for beam losses (i.e., beam is accelerated for $\simeq$ 1/2 sec, so tw is taken to be 0.5 sec), and t_f is the time at which the run ended, then

$$\langle r(\phi,\epsilon)\rangle = \frac{\sum_n r\ (\phi,\epsilon,n)\ \cdot\ \ln\ (1 + \frac{t_w}{t_f - t_n}\ )}{\sum_n \ln\ (1 + \frac{t_w}{t_f - t_n}\ )}\ .$$

2. Beam Losses

The absolute amount of beam lost is measured using a beam current transformer in HEBT, a beam current transformer in the AGS ring, and an ionization chamber (which the beam passes through) located 10 feet from the F18 main magnet (in the SEB switchyard). These are called, respectively, NX355, L20 CBM, and CE010 SEC. The approximate calibration differences have been taken into account. A program was written which sampled these devices at relevant times as well as other scalers (AGS rep - rate, linac pulse width, etc.). A batch file was written which ran this program every hour for the length of the run. From this information the amount of beam lost at different times in the cycle was measured. A single measurement is called $\xi\ (\epsilon,m)$, which is measured M times in a run. The weighted average beam loss for the run is then,

$$\langle \xi(\epsilon) \rangle = \frac{\sum_m \xi(\epsilon, m) \cdot R_m}{\sum_m R_m}$$

where R_m is defined in the same manner as R_n.

The measured beam loss distribution around the AGS ring is then,

$$\langle \xi(\phi, \epsilon) \rangle = \langle \xi(\epsilon) \rangle \cdot \frac{\langle r(\phi, \epsilon) \rangle}{\sum_\phi \langle r(\phi, \epsilon) \rangle} .$$

Unfortunately, since the amount of material between a point of a beam loss and the point at which scattered particles interact with the ionization chamber is not a constant, the above relationship does not tell us the whole story. The variations in the amount of absorber will cause variations in the measured loss in the ionization chambers. This will show up in the values of k in the activation formula. These variations should show up systematically in the distribution of k around the ring (due to the periodicity of the AGS).

Table I shows the $\langle \xi(\epsilon) \rangle$ for the two runs.

Table I
Values of $\langle \xi(\epsilon) \rangle$

Run	Irrad. T (Hours)	Cool t (Hours)	Inject. (200 MeV - 1 GeV) p/hr	Trans. (8 Gev) p/hr	Ext. (24 GeV) p/hr
Jan '87	455	5.75	1.9×10^{16}	8.3×10^{14}	3.4×10^{14}
Apr '88	1000	46.0	2.8×10^{16}	1.2×10^{15}	6.0×10^{14}

Figures 6 - 11 show the beam loss distributions at different energies for both runs.

V. COMPARING BEAM LOSS DATA TO ACTIVATION

1. General Solution

From Sections III and IV and the data presented, we now have values for $h_{act}(\phi)$ and $\langle\xi(\phi,\epsilon)\rangle$. The problem now is how do these values compare? At a particular point ϕ, the activation should be

$$D(\phi) = \sum_{i=\epsilon} k(i) \cdot \langle\xi(\phi,i)\rangle \cdot R.$$

As noted in Section IV-2, the value of k will vary with the changing thicknesses of material around the ring. If these variations are systematic such that they can be normalized out then we can include a function $g(\phi,E)$ which has the property

$$\sum_{\phi} \frac{1}{g(\phi,\epsilon)} = 1.$$

{$g(\phi,\epsilon)$ is an independent variable of k but not E}

so

$$D(\phi) = \sum_{i=\epsilon} \frac{k(i)}{g(\phi,i)} \cdot \langle\xi(\phi,i)\rangle \cdot R.$$

Since $\langle\xi(\epsilon)\rangle$ is said to occur only at three particular energies in the acceleration cycle, then all other terms are zero and we can say;

$$D(\phi) = \frac{k(\epsilon_1)}{g(\phi,\epsilon_1)} \cdot \langle\xi(\phi,\epsilon_1)\rangle \cdot R + \frac{k(\epsilon_2)}{g(\phi,\epsilon_2)} \cdot \langle\xi(\phi,\epsilon_2)\rangle \cdot R$$

$$+ \frac{k(\epsilon_3)}{g(\phi,\epsilon_3)} \cdot \langle\xi(\phi,\epsilon_3)\rangle \cdot R$$

Because of the symmetry of the AGS, we can safely say that the problem reduces to n equations with $3n/12 + 3$ unknowns. If $g(\phi,\epsilon)$ is not dependent on energy, then there are $n/12 + 3$ unknowns. For 120 monitors we can have as many as 33 unknowns!

2. Dealing With the Real World

Not only do beam losses occur only at three specific energies (or, more generally, only at three times in the acceleration cycle), but they also only occur at specific points around the machine. This has the consequence of reducing the number of equations while the number of unknowns remains the same. Also, to say the loss occurs only at a specific energy means it occurs over a finite range of energies where it is taken to occur at some average energy. The ambiguity of the average is largest at injection where an injection loss is taken to include capture and early acceleration also. Since these processes occur at a low $\partial B/\partial t$ we can safely lump them into a single category (even though the energy change is from 200 MeV to $\simeq$ 1 GeV, the uncertainties are large enough to not allow finer resolution).

A wrench is thrown into the works by the placement of the ionization monitors themselves. Although the factor $g(\phi,\epsilon)$ is intended to make this placement invarient, there are two areas where this simply is not possible, and they must be considered independently. These two points are where the injection and extraction beam lines come into the machine. At these positions, the amount of shielding between a loss in the beam line and the ionization monitor on the magnet girders in the ring is reduced to almost zero. Also, the distance from the point of a loss to the monitor is not a constant, thus making the signal very nonlinear with absolute loss.

3. Data Analysis

1. Uncertainties

A. H.P. Added Activations

Solving for $\delta h_{act}(\phi)$ {Appendix I} it is found that values of $\% \ \delta h_{act}(\phi)/h_{act}(\phi)$ varied from $\pm$ 50% to $> \pm$ 600 %. The larger values of percentages were found to be in areas of very small actual dose. Figure A3 is a plot of the frequency of an uncertainty (rounded to tens of percentages) versus the uncertainty for the January 1987 added activation. This plot shows a very skewed distribution. A standard average cannot apply to give the average uncertainty of a measurement. A correlation of percentage uncertainty to activation shows that areas of uncertainties > 200% all had activations < 10 mR (Fig. A4). From the skewed frequency distribution the mean (or median) percentage uncertainty is approximately $\pm$ 75 - 80% for both the January 1987 and April 1988 runs. In the analysis of the data values of k/g were considered only in areas of > 10 mR.

B. Beam Losses

The computed standard deviations for the weighted average RLRM data shows for all three energies that the % standard deviations vary from ± 100% to up to ± 1000%. A plot of the % standard deviations versus RLRM magnitudes shows the deviations below 10 RLRM counts quickly rise to very large values (Figs. A5, A6, A7, and A8). A comparison of the weighted average standard deviations to a normal average standard deviation shows they are approximately the same (the normal average standard deviations are, on average, greater by about ± 20%). Obviously the variations in losses seen by the RLRM are very large from day to day (the total sample sets consisted of approximately 50 samples of each RLRM monitor, at best one would expect ± 15% uncertainties). Because of the large standard deviations below 10 RLRM counts, data points below 10 counts were subtracted from the data sets.

The scaler uncertainties (weighted average) for the January 1987 injection and extraction data are about ± 25%. For the transition data the standard deviation is about ± 130%! For the April 1988 data the injection and extraction standard deviations are about ± 5% while the transition standard deviations are about ± 15%.

2. Calculation of Values of k/g

Before any subtractions were made with the data, there were a total of 139 beam loss measurements in the January 1987 data set of beam loss distributions and a total of 81 beam loss measurements in the April 1988 data set. In each run there was a maximum possible number of measurements of 360. Of the 139 measurements, 89 were subtracted out; and of the 81 measurements, 51 were subtracted out. This left 50 measurements from January 1987 and 30 measurements from April 1988 with which to calculate values of k/g.

Values of k/g were calculated directly in the areas in which there was a single energy loss. From the extraction and transition data, the values of k/g can be seen to be very consistent for both the January 1989 and April 1988 runs. These are shown in Figs. 12 and 13. Table II shows the values of all the k/g's.

In the areas of multiple energy loss, the uncertainties propagate to very large values very quickly when evaluated as simultaneous equations (matrix evaluation for 2 and 3 independent variables). This did not work out well since extremely large standard deviations developed and many times the constants came out negative. What worked somewhat better was to

TABLE II: DATA

JAN 87 RATE = 4.94 APR 88 RATE = 3.31

		ACTIV. MAX	ACT/RATE MAX	losses inj.	losses trn.	losses ext.	VALUES OF k/g		
JAN	K16	113	23	1.0E+15	0	0	2.3E-14		
JAN	A14	435	88	0	2.1E+14	0		4.2E-13	
JAN	B2	227	46	0	8.8E+12	0		5.2E-12	
JAN	B4	77	16	0	6.0E+12	0		2.6E-12	
JAN	B6	167	34	0	1.4E+13	0		2.4E-12	
JAN	B14	13	3	0	7.0E+12	0		3.6E-13	
JAN	B18	38	8	0	2.1E+13	0		3.6E-13	
JAN	E6	83	17	0	1.3E+13	0		1.3E-12	
JAN	G14	45	9	0	6.4E+12	0		1.4E-12	
JAN	H6	90	18	0	1.3E+13	0		1.4E-12	
JAN	I2	182	37	0	1.2E+13	0		3.1E-12	
JAN	L10	203	41	0	5.9E+12	0		7.0E-12	
JAN	L12	143	29	0	4.7E+13	0		6.1E-13	
JAN	L14	36	7	0	1.1E+13	0		6.7E-13	
JAN	L16	15	3	0	8.5E+12	0		3.5E-13	
APR	H6	140	42	0	1.7E+13	0		2.4E-12	
JAN	C6	25	5	0	0	1.2E+12			4.2E-12
JAN	I16	25	5	0	0	3.2E+12			1.6E-12
APR	G16	25	8	0	0	4.5E+12			1.7E-12
APR	G18	26	8	0	0	6.3E+12			1.2E-12
APR	H16	31	9	0	0	4.0E+12			2.3E-12
APR	I14	71	21	0	0	1.3E+13			1.7E-12
APR	I16	46	14	0	0	1.0E+13			1.3E-12
JAN	A16	149	30	5.6E+15	4.9E+13	0	1.2E-16	6.2E-13	
JAN	A20	1742	352	1.1E+15	9.6E+12	0	3.2E-13		
JAN	A18	57	12	2.1E+15	1.5E+13	1.4E+12	1.0E-16	6.2E-13	
JAN	E18	164	33	1.3E+15	1.4E+13	1.5E+13	1.9E-16		2.2E-12
JAN	E20	2441	494	2.7E+15	6.4E+13	1.3E+13			3.8E-11
JAN	F2	529	107	1.1E+15	1.1E+14	1.8E+13			5.9E-12
JAN	F4	157	32	0	1.2E+13	1.4E+12			2.3E-11
APR	E18	65	20	0	1.3E+13	1.4E+13			1.4E-12
APR	E20	1291	390	8.9E+15	1.8E+14	7.8E+13			5.0E-12
APR	F2	835	252	8.7E+15	5.9E+14	1.2E+14			2.0E-12
APR	F4	243	73	0	1.0E+14	2.3E+13			3.2E-12
JAN	F6	1347	273	0	2.1E+13	1.4E+14			1.9E-12
APR	F6	844	255	4.7E+15	6.4E+13	1.4E+14			1.9E-12
JAN	F8	202	41	0	3.9E+13	1.4E+13			2.9E-12
APR	F8	567	171	0	2.6E+13	1.1E+13			1.6E-11
JAN	F10	272	55	0	0	5.4E+12			1.0E-11
APR	F10	85	26	0	1.7E+13	1.8E+13			1.4E-12
JAN	F12	131	26	0	2.1E+13	5.7E+13			4.6E-13
APR	F12	75	23	0	0	2.9E+10			7.8E-10
JAN	F14	278	56	0	5.8E+12	1.1E+13			5.1E-12
APR	F14	212	64	0	3.6E+13	2.0E+13			3.2E-12
JAN	F18	83	17	0	8.5E+12	1.6E+13			1.1E-12
APR	F18	72	22	0	3.6E+13	3.1E+13			7.0E-13
JAN	F20	92	19	0	0	1.7E+13			1.1E-12
APR	F20	52	16	0	0	3.5E+13			4.5E-13
JAN	G2	74	15	0	0	1.7E+13			8.8E-13
APR	G2	55	16	0	0	2.4E+13			6.8E-13

take average values of k/g from single energy loss data and calculate out a single constant from a multiple energy loss point (i.e., used average k/g from transition data to calculate injection k/g in areas of injection and transition losses). This procedure was necessary for the injection data since there was only a single point at which there was only injection loss measured. Out of the ten measured injection losses only 5 values of k/g were obtained. The standard deviation in these is large. Figure 14 shows the constants calculated for injection data.

For the transition and extraction data, areas of multiple energy loss were treated differently. The assumption made was that the contribution to the activation in a particular area from the lower energy losses was less significant than from the highest energy loss and so considered negligible within the uncertainties. The values of k/g obtained for transition and extraction were consistent with the values obtained from the single energy loss data. Figures 15 and 16 show the values of all the k/g's obtained.

Finally, the section of the AGS from which beam is extracted was considered separately (from E18 to G4). Values of k/g were calculated in these areas assuming only extraction losses. Figure 17 shows the resulting values. Of these measurements, five are shown in red due to bad, or suspected bad, beam loss measurements. The determination of whether a particular monitor was reading properly or not is somewhat ambiguous. For this reason, I take the position that if a particular monitor deviated largely from the normal, it was to be considered suspicious. The criterion for determining what is or is not normal is where the ambiguities arise. The criterion used was to assume that in the two runs, the mechanism for a particular loss was basically the same and so the ratios of beam loss in a particular area should be about the same. If the ratios were largely different, then one of the monitors was considered bad (reading small losses in an area of large dose). The five monitors found to be largely inconsistent using this method were:

January 1987	E20
	F4
	F10
April 1989	F8
	F12

TABLE III

Average Values of k/g, k, and g

	US k/g	DS k/g	k	US g	DS g
Trans.	3.2×10^{-12}	6.0×10^{-13}	5.1×10^{-13}	6.3	1.2
(± Stand. Dev.)	$\pm 1.8 \times 10^{-12}$	$\pm 3.1 \times 10^{-13}$	$\pm 2.6 \times 10^{-13}$	±4.1	±0.1
Extract.	4.5×10^{-12}	1.6×10^{-12}	1.2×10^{-12}	3.7	1.4
(± Stand. Dev.)	$\pm 1.1 \times \pm 10^{-12}$	$\pm 3.5 \times 10^{-13}$	$\pm 2.5 \times 10^{-13}$	±0.9	±0.1

3. Values of k and g

From Figs. 13, 14, 15, and 16 it can be seen that there are large differences between values of k/g in the US and DS halves of a superperiod. If these differences are due to geometry then it appears at least two values of g can be obtained for each energy. The justification for the US being different from the DS is that the US main magnets have their backlegs facing to the outside of the AGS ring while the DS main magnets have their backlegs facing toward the inside of the AGS ring. All the RLRM monitors subtend along the main magnet girders along the outside of the AGS ring. If there is more material between the point of a loss and the point at which the scattered flux intersects an ionization chamber, then the expected signal from the chamber would be smaller, thus making ξ smaller and giving a larger value for k/g. This is consistent with what is observed in Figs. 13, 14, 15, and 16. Table III (p. 19) summarizes the average values obtained for k/g, k, and g for transition and extraction.

Obtaining values of g for injection is not possible from the data in the January 1987 and April 1988 runs since values of k/g were obtained only in DS sections.

In previous notes[3 - 5] values of k were obtained but with a much different method. It is of interest though, how they compare. The previous values obtained were:

$$k_i = 5 \times 10^{-14} \pm 2.5 \times 10^{-14} \text{ R/p/sec.}$$
$$k_t = 4 \times 10^{-12} \pm 2.0 \times 10^{-12} \text{ R/p/sec.}$$
$$\text{and} \quad k_e = 7 \times 10^{-12} \pm 3.5 \times 10^{-12} \text{ R/p/sec.}$$

in the new units these are

$$k_i = 1.4 \times 10^{-14} \text{ mR/proton}$$
$$k_t = 1.1 \times 10^{-12} \text{ mR/proton}$$
$$\text{and} \quad k_e = 2.0 \times 10^{-12} \text{ mR/proton.}$$

Table IV

Values of k

	US k/g	DS k/g	k	Prev. k's
Inj.*		5.8×10^{-15} $\pm 9.8 \times 10^{-15}$		1.4×10^{-14}
Tran.	3.2×10^{-12}	6.0×10^{-13}	5.1×10^{-13}	1.1×10^{-12}
Ext.**	4.5×10^{-12}	1.6×10^{-12}	1.2×10^{-12}	2.0×10^{-12}

*A20 not included.
**Extract region not included.

Recall from Sec. II.3 the calculated value is 5.3×10^{-14} mR/p.

VI. OTHER TECHNIQUES IN THE STUDY OF ACTIVATIONS

In this section, I will summarize the techniques used at CERN as outlined by Y. Baconnier[9].

If the energy deposited by losses is W, integrated over the duration of a run T, is

$$W = \frac{N_l \cdot q \cdot V}{2\pi R}$$

where N_l is the number of particles lost, q is the fundamental unit of charge, eV is the energy of the particles lost, and $2\pi R$ is the circumference of the accelerator. The instantaneous power deposited during the run is then

$$P = \frac{W}{T} .$$

Calling k_a the ratio of the total dose to the energy deposited;

$$k_a = \frac{P}{W} , \quad (Gy \cdot m/J)$$

then k_a has the units of m/kg. If $1/k_a$ is 200 kg/m (in the PS) then the surface dose can be estimated by assuming that the energy W is deposited in a mass $1/k_a$ of 200 kg/m of vacuum chamber.

The relation between the power deposited P and the dose rate D due to induced radioactivity is

$$D = k \cdot P \log \left(\frac{T + t}{t}\right).$$

Note that in this treatment the energy dependence is now in the factor P (not k), so obviously it assumes that the measured dose is directly proportional to the energy of the beam loss.

Table V shows the comparison of the AGS to the CERN PS using the above treatment (the AGS data is from the January 1987 run). The AGS equivalent to PS data is just the AGS data equated with the same T as the PS data.

The AGS, given the same length of running time as the PS but with losses unchanged, deposited (to activation) 2.8 times more power than the CERN PS! Note that given the same amount of running time the ratio of P/W for the CERN PS and for the AGS is the same!

Because of how Y. Baconnier treats the above expression for D, comparison between the CERN k (which is independent of energy, assuming Dose is directly proportional to deposited power) and the k derived in this report (which assumes deposited power cannot be measured from beam loss alone) is not possible. Fortunately, he provides enough data in his report to allow us to come up with k's from beam loss. Based on his Table AII,[9] which provides data for losses and % dose (based on power deposited) at different energies, I made up the following table. The data from the CERN PS agree's very well with the AGS.

TABLE V

Average Values of k/g, k, and g

	US k/g	DS k/g	k	US g	DS g
Trans.	3.2×10^{-12}	6.0×10^{-13}	5.1×10^{-13}	6.3	1.2
(± Stand. Dev.)	$\pm 1.8 \times 10^{-12}$	$\pm 3.1 \times 10^{-13}$	$\pm 2.6 \times 10^{-13}$	±4.1	±0.1
Extract.	4.5×10^{-12}	1.6×10^{-12}	1.2×10^{-12}	3.7	1.4
(± Stand. Dev.)	$\pm 1.1 \times \pm 10^{-12}$	$\pm 3.5 \times 10^{-13}$	$\pm 2.5 \times 10^{-13}$	±0.9	±0.1

TABLE VI
Values of k for CERN PS

Process	Energy	Beam Loss (P/hr)	Dose (mRem)	k (for the rate of 5.017)
Injection	0.8 GeV	1.69×10^{15}	893	1.1×10^{-13} mR/p
Start-up	15 GeV	9.5×10^{12}	94	2.0×10^{-12} mR/p
Development	15 GeV	2.3×10^{13}	235	2.0×10^{-12} mR/p
Transfer	14 GeV	2.7×10^{14}	2538	1.9×10^{-12} mR/p
Slow Extract	24 GeV	4.2×10^{12}	47	2.2×10^{-12} mR/p
Fast Extract	26 GeV	4.9×10^{13}	893	3.6×10^{-12} mR/p

IX. CONCLUSIONS

The constants required to predict residual activity using the Sullivan - Overton relationship have been found. Although the uncertainties are large, they are manageable and it should be possible to predict activity based on beam losses and beam loss distributions. Table VII summarizes the values of k found and how they compare to previous studies and to values determined from data from the CERN PS.

Table VII

Summary of Values of k

Energy (GeV)	k (this report) (mR/p)	previous k's (mR/p)	CERN k's (mR/p)
0.2	5.8×10^{-15}	1.4×10^{-14}	----
0.8	----	-----	1.1×10^{-13}
8.0	5.1×10^{-13}	1.1×10^{-12}	----
14.0	----	-----	1.9×10^{-12}
15.0	----	-----	2.0×10^{-12}
24.0	1.2×10^{-12}	2.0×10^{-12}	2.2×10^{-12}
26.0	----	-----	3.6×10^{-12}

An understanding of the RLRM system has been greatly improved, although more questions have arisen. Differences in the response of radiation monitors in different locations have been measured and it has been shown that the monitors do respond differently to the same amount of loss depending on their location. At high energies there appears to be at least a factor of 2 difference between monitors in the upstream and downstream

halves of a superperiod. At lower energies this factor appears to get even larger. Table VIII summarizes our values of g.

Table VIII
Summary of values of g

Energy (GeV)	g (US halves)	g (DS halves)
8.0	6.3 ± 4.1	1.2 ± 0.1
24.0	3.7 ± 0.9	1.4 ± 0.1

Sections III, IV, and V demonstrate what is required to accurately compare residual activation measurements to measurements of beam loss distributions. These sections likewise demonstrate what is required to reasonably predict activation. Section VI showed how the CERN PS compares to the AGS. Certainly the PS is much cleaner but with the present upgrades being made in the AGS, the two machines will be very similar very soon.

There is certainly room for further work in this study. Effort to bring the uncertainties and standard deviations down is imperative. The complex geometry of accelerators is going to present the limiting factor on the uncertainties. No matter how well one can measure the amount of beam lost at a particular point, the complex nature of the radiation field will make accurate predictions very difficult.

Steve Musolino has suggested a simple experiment which should get done. This is the measurement of the decay rate in a few different areas in the AGS ring. A comparison of the measured rate to the Sullivan - Overton rate would be invaluable.

I was initially surprised with the uncertainties found in the RLRM data. Certainly, the system was not originally designed to be used in this manner. I must admit that one possible source to he large uncertainties could be in the methods of averaging. It is better to compute the beam lost per 3° weighted average than it is to compute the weighted average of the RLRM conts and total beam lost and then compute the weighted average beam lost per 3°. The final results would not be much different but the propagation of the uncertainties might be slower since he RLRM counts would be normalized to actual loss before being weighted to the decay rate. In practice, this method is much more time consuming, which is why it was not done in the first place.

Acknowledgements

I would like to thank W.R. Casey, G. Bennett, J.W. Glenn, E. Bleser, S. Musolino, S. Tanaka and P. Golon for their comments and assistance. They are each invaluable sources of knowledge. I would like to thank P. Carolan for helping out in writing some of the computer programs used in the data collection and summary. I would like to thank the MCR operations and H.P. technicians for their assistance in the data collection. I would also like to thank Barbara Cox who patiently typed this paper into her P.C. (this was done in Totalword).

APPENDIX I

I. HP SURVEY UNCERTAINTIES

A. Quantitative Demonstration of Errors in H.P. Measurements

The uncertainty in a single measurement has a number of sources:

1. Measuring device accuracy. For the H.P. probes, it is approximately 10%

2. The instrument has a "μsec" time constant. The uncertainty is a function of dose-rate.

These two uncertainties are basically the same since the scale is made to the accuracy of the device.

3. Uncertainty in positioning the point of a measurement (measurement error).

The only way to reduce this kind of uncertainty is to take a large number of samples and reduce the uncertainty to statistical variations. This cannot be done in the present system since the dose a technician would pick up could be significant.

This uncertainty can be estimated, though, based on measurements made by Gilbert & Thomas in the early 1970's of the distribution of dose around an AGS main magnet, (taken from Accelerator Health Physics by H. Patterson & R. Thomas, p. 516). Figures 26 and 27 demonstrate the data. Figure 26 shows that the dose falls off by a $\simeq$ 1/r relationship in the radial direction from the center of the magnet in the open side. For a 12" $\pm$ 1" measurement the uncertainty is approximately $\pm$ 5%. Figure 27 shows the magnet shielding has a large effect on the vertical dose distribution. For a vertical position uncertainty of $\pm$ 6" (this uncertainty is due to the angle in which the H.P. tech holds the meter which varies from person to person), the dose uncertainty will be $\simeq$ 50%. Since the measurements are not made at the middle of the main magnets (but at the ends), this distribution in the vertical dose is probably not so narrow and the uncertainty is smaller.

To quantify all these uncertainties is difficult because little detailed data exists on it. Based on the observations and with interviews of H.P. techs, it will be assumed in this report that the confidence level in the H.P. measurements is $\pm$ 50%.

II. Beamloss Uncertainties

The RLRM and beam loss data are each dominated by systemic uncertainties. The standard deviation in $\langle r(\phi,\epsilon)\rangle$ is

$$S(\langle r(\phi,\epsilon)\rangle) = \left[\frac{\sum_n (r(\phi,\epsilon,n) - \langle r(\phi,\epsilon)\rangle)^2 \cdot R_n}{\sum_n R_n} \right]^{1/2}$$

the standard deviation in $\langle \xi(\epsilon)\rangle$ is

$$S(\langle \xi(\epsilon)\rangle) = \left[\frac{\sum_m (\xi(\epsilon,m) - \langle \xi(\epsilon)\rangle)^2 \cdot R_m}{\sum_m R_m} \right]^{1/2}$$

III. Activation Uncertainties

The uncertainties for the H.P. surveys were calculated using

$$\delta h_{act}(\phi)^2 = \left\{ \frac{\partial h_{act}(\phi)}{\partial h_3} \right\}^2 \cdot \delta h_3^2 + \left\{ \frac{\partial h_{act}(\phi)}{\partial h_3'} \right\}^2 \delta h_3'^2$$

where

$$\delta h'^2_3 = \left\{\frac{\partial h'_3}{\partial C_{eff}}\right\}^2 \delta C_{eff}{}^2 + \left\{\frac{\partial h'_3}{\partial T_{eff}}\right\}^2 \delta T_{eff}{}^2$$

$$+ \left\{\frac{\partial h_3}{\partial (t_3 - t_0)}\right\}^2 \cdot \delta (t_3 - t_0)^2$$

$$\delta C_{eff}{}^2 = \left\{\frac{\partial C_{eff}}{\partial h_2}\right\}^2 \cdot \delta h_2^2 + \left\{\frac{\partial C_{eff}}{\partial T_{eff}}\right\}^2 \delta Teff^2$$

$$+ \left\{\frac{\partial\ C_{eff}}{\partial (t_2 - t_0)}\right\}^2 \cdot \quad \delta (t_2 - t_{\ 1})^2$$

$$\delta T_{eff}{}^2 = 2 \cdot \left[\left\{\frac{\partial T_{eff}}{\partial (t_1 - t_0)}\right\}^2 \cdot \delta (t_1 - t_0)^2 \right.$$

$$\left. + \left\{\frac{\partial T_{eff}}{\partial (t_2 - t_0)}\right\}^2 \cdot \delta (t_2 - t_0)^2 \right]$$

$$+ \left\{\frac{\partial T_{eff}}{\partial h_1}\right\}^2 \delta h_1^2 + \left\{\frac{\partial T_{eff}}{\partial h_2}\right\}^2 \cdot \delta h_2^2$$

The uncertainties for the April 1988 run were modified for the extra H.P. survey, but they are basically the same form as these.

APPENDIX II

LEAST SQUARES CALCULATION AND χ^2 FITS

The least squares condition for

$$\sum_{\phi} \left[h_{act}(\phi) - \left\{\sum_{i=\epsilon} \frac{k(i)}{g(\phi,i)} \cdot \langle\xi(\phi,i)\rangle \cdot R\right\}\right]^2 = M,$$

is

$$\frac{\partial M}{\partial \kappa(\phi,\epsilon)} = 0, \text{ where } \kappa(\phi,\epsilon) = \frac{k(\epsilon)}{g(\phi,\epsilon)} .$$

Then, (rigorous notation ignored for simplifying long relationship).

$$\langle\kappa(\phi,\epsilon_1)\rangle =$$

$$\frac{\sum_{\phi} h\xi(\epsilon_1)\cdot R - \sum_{\phi}\kappa(\epsilon_2)\xi(\epsilon_1)\cdot\xi(\epsilon_2)\cdot R^2 - \sum_{\phi}\kappa(\epsilon_3)\cdot\xi(\epsilon_1)\cdot\xi(\epsilon_3)\cdot R^2}{\sum_{\phi}\{\xi(\epsilon_1)\cdot R\}^2}$$

For transition and extraction, since lower energy contributions are ignored, this simplifies to

$$\langle\kappa(\phi,\epsilon)\rangle = \frac{\sum_{\phi} h_{act}(\phi) \cdot \langle\xi(\phi,\epsilon)\rangle \cdot R}{\sum_{\phi}\{\langle\xi(\phi,\epsilon)\rangle \cdot R\}^2}$$

the chi-square test, or the goodness of this fit is;

$$\chi^2 = \frac{\sum_{\phi}\left[h_{act}(\phi) - \langle\kappa(\phi,\epsilon)\rangle \cdot \langle\xi(\phi,\epsilon)\rangle \cdot R\right]^2}{\sum_{\phi}\{\langle\kappa(\phi,\epsilon)\rangle \cdot \langle\xi(\phi,\epsilon)\rangle \cdot R\}}$$

Table IX summarizes the results.

Table IX

Values of $<\kappa(\phi,\epsilon)>$ and χ^2

	US κ	US χ^2	DS κ	DS χ^2
Inj.	----	-----	6.7×10^{-15}	67.1
Tran.	2.5×10^{-12}	40.7	4.4×10^{-13}	7.0
Ext.	4.8×10^{-12}	30.3	1.5×10^{-12}	23.8

APPENDIX III

I. Exponential Integral Functions[11]

These are an example of an asymptotic series. The nth integral $En(\chi)$ for positive real arguments is defined by

$$En(\chi) = \int_1^\infty e^{-\chi t} \frac{dt}{t^n}$$

$$= \int_0^1 e^{-\chi/\mu} \mu^{n-1} \frac{d\mu}{\mu}$$

When defined in this way, they satisfy the recursion formulae: (prime denotes differentiation with respect to χ).

$$nE_{n+1}(\chi) = e^{-\chi} - \chi\, En(\chi) \qquad (n \geq 1)$$

$$E'_{n+1}(\chi) = -En(\chi) \qquad (n \geq 1)$$

and $$E'_1(\chi) = -\frac{e^{-\chi}}{\chi}$$

so all exponential integrals can be reduced to the first exponential integral

$$E_1(\chi) = -E_i(-\chi) = \int_1^\infty e^{-\chi t} \frac{dt}{t} = \int_\chi^\infty e^{-t} \frac{dt}{t}$$

For large values of χ an asymptotic expansion for $E_1(\chi)$ can be found. By continuing the process

$$E_1(\chi) = -\int_\chi^\infty \frac{d}{dt}(e^{-t}) \frac{dt}{t} = \frac{e^{-\chi}}{\chi} + \int_\chi^\infty \frac{d}{dt}(e^{-t}) \frac{dt}{t^2}$$

then it is found that

$$E_1(\chi) = \frac{e^{-\chi}}{\chi} \left[1 - \frac{1}{\chi} + \frac{2}{\chi^2} - \frac{6}{\chi^3} + \cdots\right]$$

For $\chi \to 0$, $E_1(\chi)$ has a logarithmic singularity, and a series expansion can be found.

$$E_1(\chi) = \int_1^{\infty} e^{-t} \frac{dt}{t} + \int_{\chi}^{1} e^{-t} \frac{dt}{t}$$

$$= \{\int_1^{\infty} e^{-t} \frac{dt}{t} - \int_0^{1} (1-e^{t}) \frac{dt}{t} \} + \int_{\chi}^{1} \frac{dt}{\chi} + \int_0^{\chi} (1-e^{-t}) \frac{dt}{t}$$

then

$$E_1(\chi) = - \gamma - \ln(\chi) + \int_0^{\chi} (1 - e^{-t}) \frac{dt}{t}$$

where $\gamma = 0.5772156 \ldots$ is the Euler - Mascheroni constant. The integral has a convergent series expansion for $\chi \to 0$. Then

$$E_1(\chi) = - \gamma - \ln(\chi) - \sum_{n=1}^{\chi} (-1)^n \frac{\chi^n}{n \cdot n!} .$$

APPENDIX IV

LIST OF SYMBOLS

Section II

D	Dose rate from induced radioactivity mR/hr.
k	Sullivan - Overton constant mR/proton.
ξ	Number of high energy protons per interaction.
T	Irradiation time
t	Cool down time
$N\nu$	Number of radioactive nuclei of ν produced per unit volume per unit time.
Φ	Flux of incident particles (# particles/cm^2 sec)
N_T	Number of target atoms per unit volume.
$\sigma_{T,\nu}$	Cross section leading from target nucleus (T) to desired isotope (ν).
ρ	Density of target.
n_ν	Number of nuclei of ν per gm of target material.
n_T	Number of target atoms per gm of target material.
N_o	Avagadros number = 6.02×10^{23} atoms/mole.
A_T	Atomic weight of target material.
t_ν	Mean-life of isotope ν.
$t_{1/2,\nu}$	Half-life of isotope ν.
t_i	Irradiation time
t_c	Cooling time
a	Total activation of target, (disintegrations/sec/gm).
λ	$1/t_\nu$
γ	Euler - Mascheroni constant = 0.5772
α	Cross sectional area of interaction of beam on target.

Section II (Continued)

$\bar{\sigma}_s$ Average isotopic production cross section.

f Fraction of isotopes that have decay constants between λ_2 and λ_1.

σ_{tot} Total production cross section.

S Gamma Activity

E Average energy of absorbed gammas.

μ Mass energy absorption coefficient.

r Distance from source of induced activity.

Q Quality factor, conversion from rad to rem.

Section III

h_1, h_2, h_3 Single act measurement taken at some time t_1, t_2, or t_3.

t_1, t_2, t_3 Times of respective HP surveys all referenced to some to.

T_{eff} Effective (not measured) irradiation time required to produce measured decay rate between surveys at times t_2 and t_1.

ξ_{eff} Effective (not measured) beam loss required to provide measured offset in dose between surveys at times t_3 and t_2.

t_b The beginning of a run which adds to the activation.

t_e The end of a run which adds to the activation.

h_3' Estimated background activation at time t_3.

h_{act} Estimated added activation from beam loss between t_e and t_b.

ξ_{be} The average beam loss (P/hr) between t_e and t_b.

Section IV

$r(\phi,\epsilon,n)$	A single beam loss measurement with ionization monitors (arbitrary units)
ϕ	Position (every 3°) at a measurement.
ϵ	Corresponding energy of beam at time of beam loss measurement.
n	The nth of N samples.
ξ_n	Beam loss at time of nth sample.
R_n	Rate of decay of activity induce by losses at time of nth sample with respect to a later time t_f corresponding to the end of irradiation.
t_n	Time of nth sample.
t_f	End of irradiation time .
t_w	For each sample n, the time interval over which beam loss occurred.
$\xi(\epsilon,m)$	A single measurement of absolute beam loss at a beam energy of ϵ (protons/hour).
m	The mth sample of M total measurements.
R_m	Same as R_n except for mth sample time.

Section V

$D(\phi)$	Measured activation at position ϕ.
$g(\phi,\epsilon)$	A normalization factor.

Section VI

W	Energy deposited by losses.
T	Irradiation time
N_e	Number of particles lost.
q	Unit of charge.
eV	Energy of particles lost.
R	Radius of Accelerator.

Section VI (Continued)

P	Instantaneous power deposited during the run.
k_a	The ratio of tot. dose to energy deposited.
D	Dose rate
t	Cool time
k	Constant of proportionality (not same k as in previous sections).

REFERENCES

1. AGS Dept. Memo from M. Tanaka on Results of Recent AGS Ring Radiation Surveys by H.P. dated 6/10/86.

2. AGS Dept. Memo from M. Tanaka on Results of H.P. Radiation Surveys dated 6/23/86.

3. Acc. Div. Tech. Note No. 264, K. Brown and M. Tanaka, Beam Induced Radioactivity Around the AGS Ring, 9/26/86.

4. AGS Studies Report No. 220, K. Brown and M. Tanaka, Latest Results from Studies of Induced Radioactivity, 2/24/87.

5. 1987 Part. Accel. Conf., K. Brown & M. Tanaka, Studies of Induced Radioactivity at the AGS, BNL No. 39325.

6. An Approximate Relation for the Prediction of the Dose Rate from Radioactivity Induced in High Energy Particle Accelerators by A.H. Sullivan, Health Physics, Vol. 23, (August 1972) pp. 253 - 255.

7. Induced Radioactivity and its Relation to Beam Losses in the CERN 26 GeV Proton Synchrotron by A.H. Sullivan. Nuclear Instruments and Methods in Physics Research A257, (1987) pp. 185 - 188.

8. Acc. Health Physics by H. Wade Patterson and Ralph H. Thomas, LBL, Univ. of Cal., Berkeley, 1973.

9. Lessons for Kaon Factories From the CERN PS by Y. Baconnier. Intern. Workshop on Hadron Fac. Tech., Sante Fe, 2/87.

10. Induced Radioactivity by Maracel Barbier, CERN, 1969.

11. Radiative Transfer, S. Chandrasekhar; Univ. of Chic., 1960.

FIGURE CAPTIONS

Fig. 1 January 1987 H.P. AGS Survey.

Fig. 2 April 1988 H.P. AGS Survey.

Fig. 3 Example of Background Activation from January 1987 data.

Fig. 4 January 1987 Added Activation for Outer Maximums/3°.

Fig. 5 April 1988 Added Activation for Outer Maximums/3°.

Fig. 6 Weighted Average Beam Losses at Injection for January 1987.

Fig. 7 Weighted Average Beam Losses at Injection for April 1988.

Fig. 8 Weighted Average Beam Losses at Transition for January 1987.

Fig. 9 Weighted Average Beam Losses at Transition for April 1988.

Fig. 10 Weighted Average Beam Losses at Extraction for January 1987.

Fig. 11 Weighted Average Beam Losses at Extraction for April 1988.

Fig. 12 Values of k/g for Single Energy Areas Versus Position in Superperiods at Transition for Both Runs.

Fig. 13 Values of k/g for Single Energy Areas Versus Position in Superperiods at Extraction for Both Runs.

Fig. 14 All Values of k/g Versus Position in Superperiods at Injection.

Fig. 15 All Values of k/g Versus Position in Superperiods at Transition for Both Runs. Single Energy Values distinguished from Multiple Energy Areas.

Fig. 16 All Values of k/g (Excluding Extraction Region) Versus Position in Superperiods at Extraction for Both Runs. Single Energy Values Distinguished from Multiple Energy Areas.

Fig. 17 Values of k/g Versus Position in Extraction Region at Extraction for Both Runs (From E18 to G4).

APPENDIX FIGURES

FIGURE 1: AGS ACTIVATION SURVEY

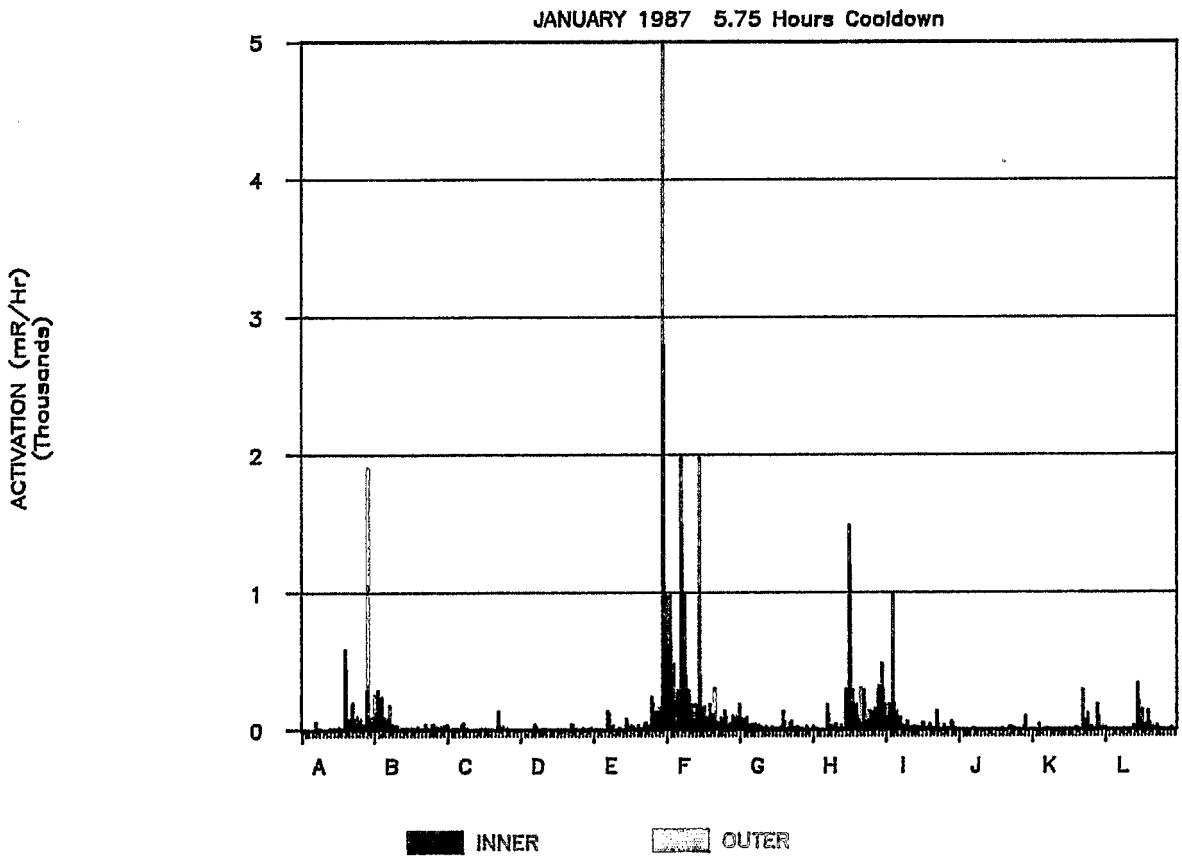

FIGURE 2: AGS RESIDUAL ACTIVATION

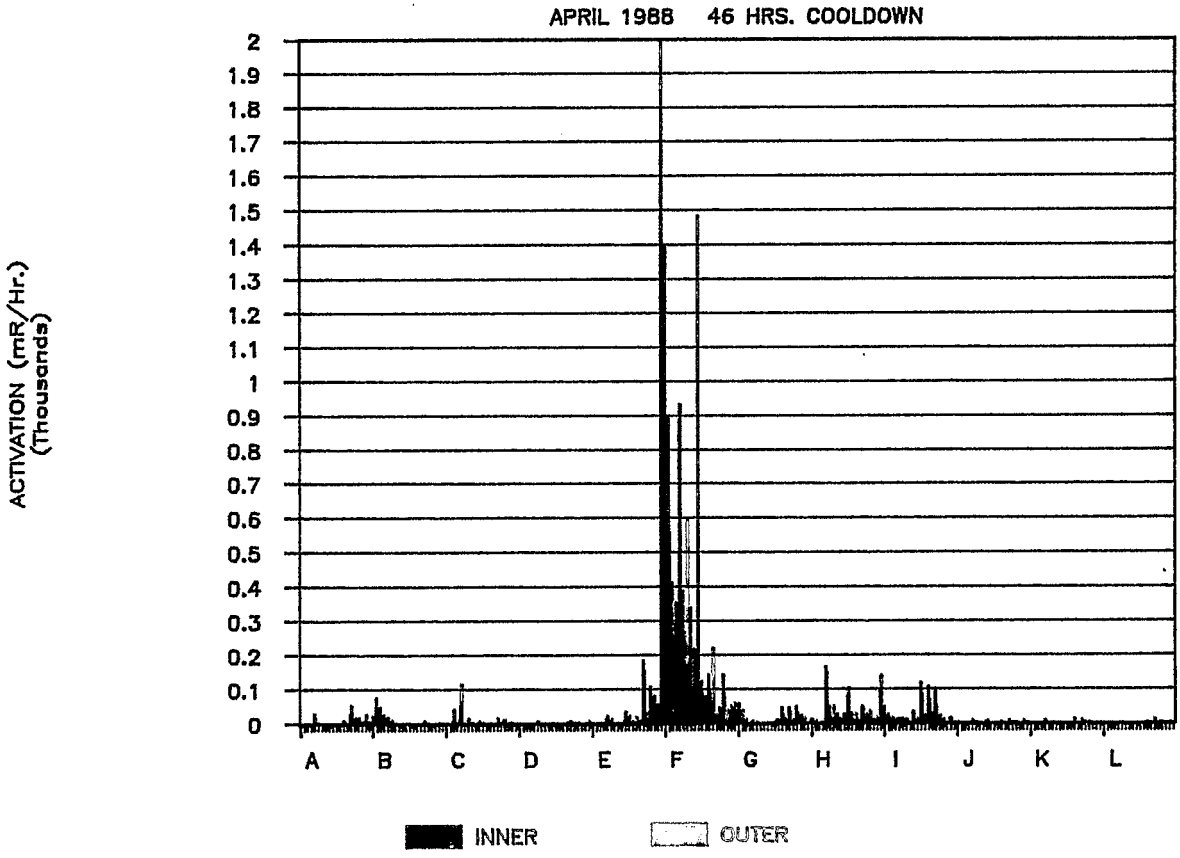

FIGURE 3: EST. BACKGROUND ACTIVATION

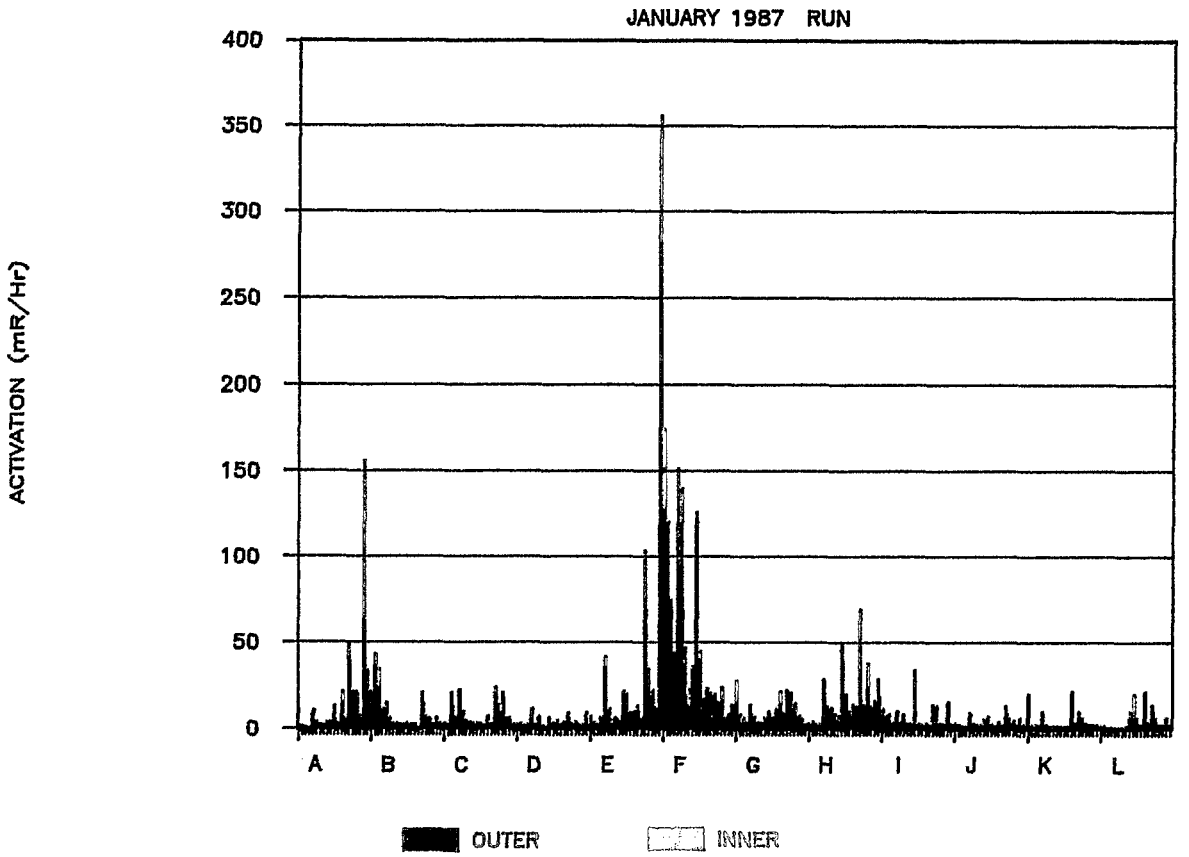

FIGURE 4: EST. ADDED ACTIVATION

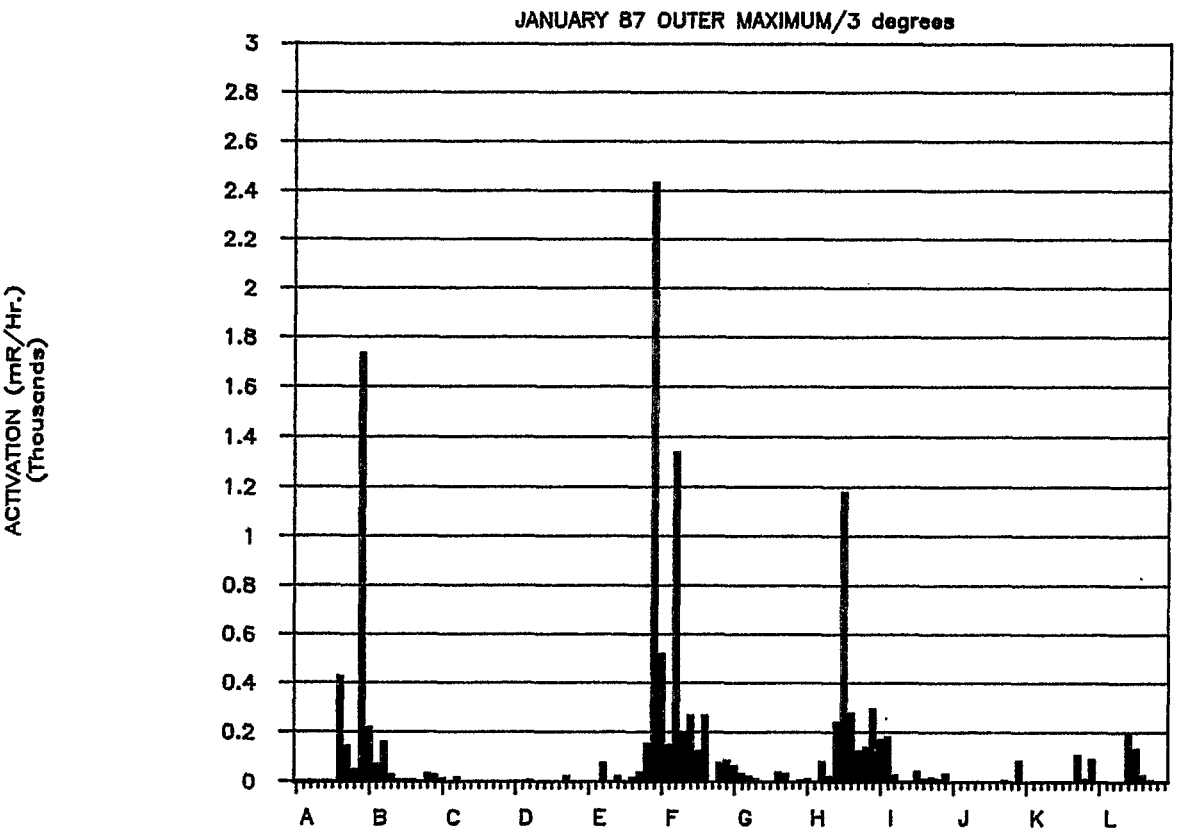

FIGURE 5: EST. ADDED ACTIVATION

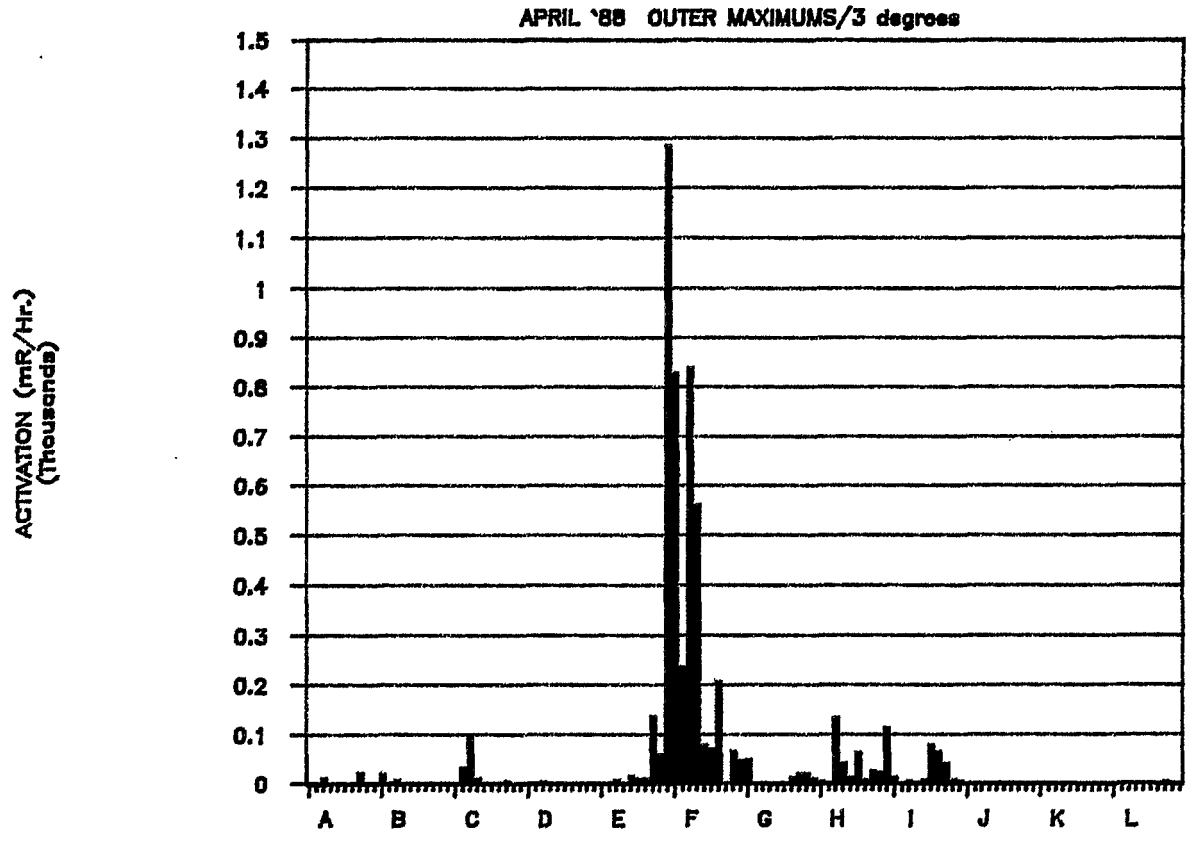

FIGURE 6: WT. AVG. LOSS DISTRIBUTIONS

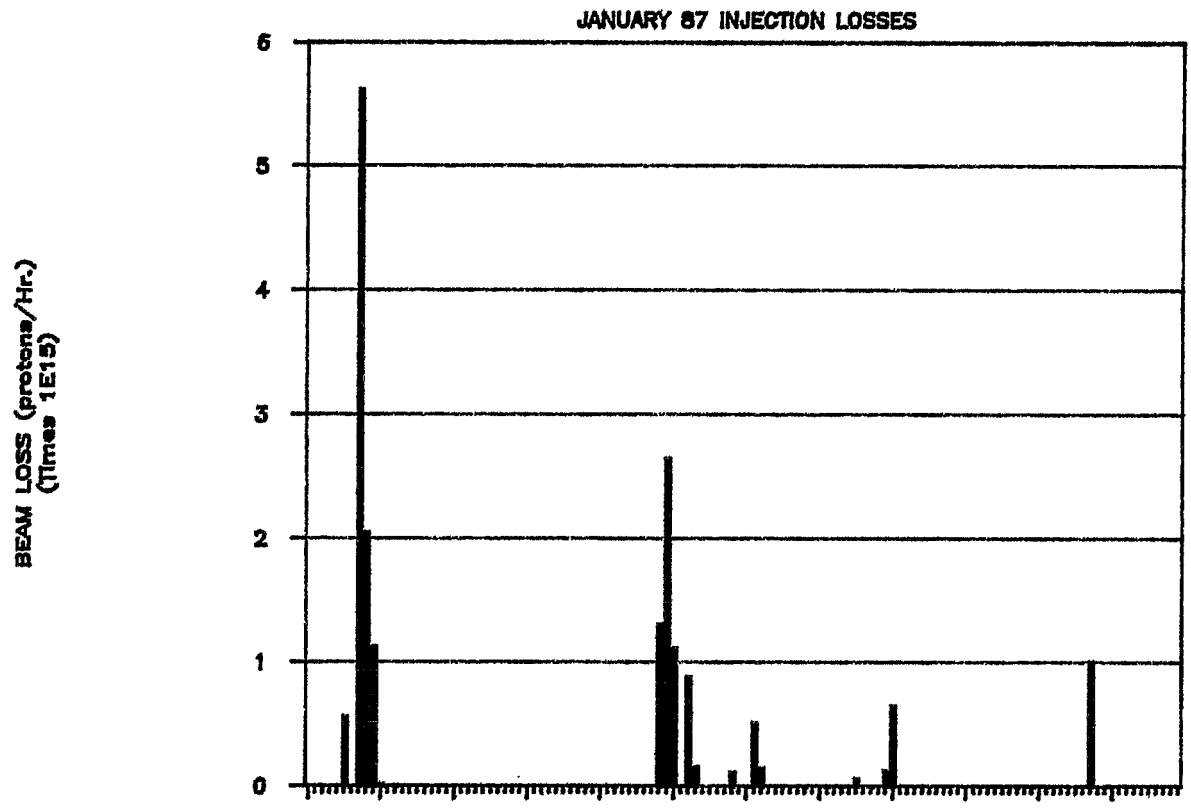

FIGURE 7: WT. AVG. LOSS DISTRIBUTIONS

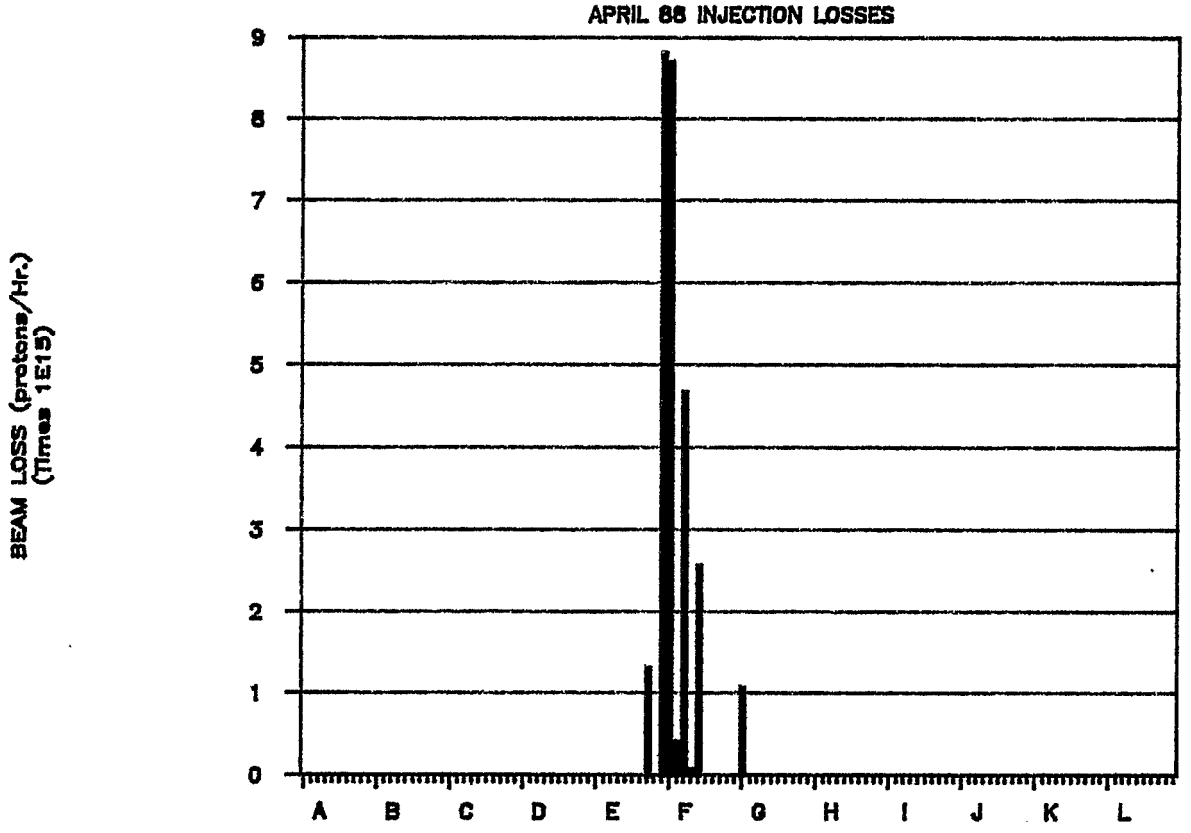

FIGURE 8: WT. AVE. LOSS DISTRIBUTIONS

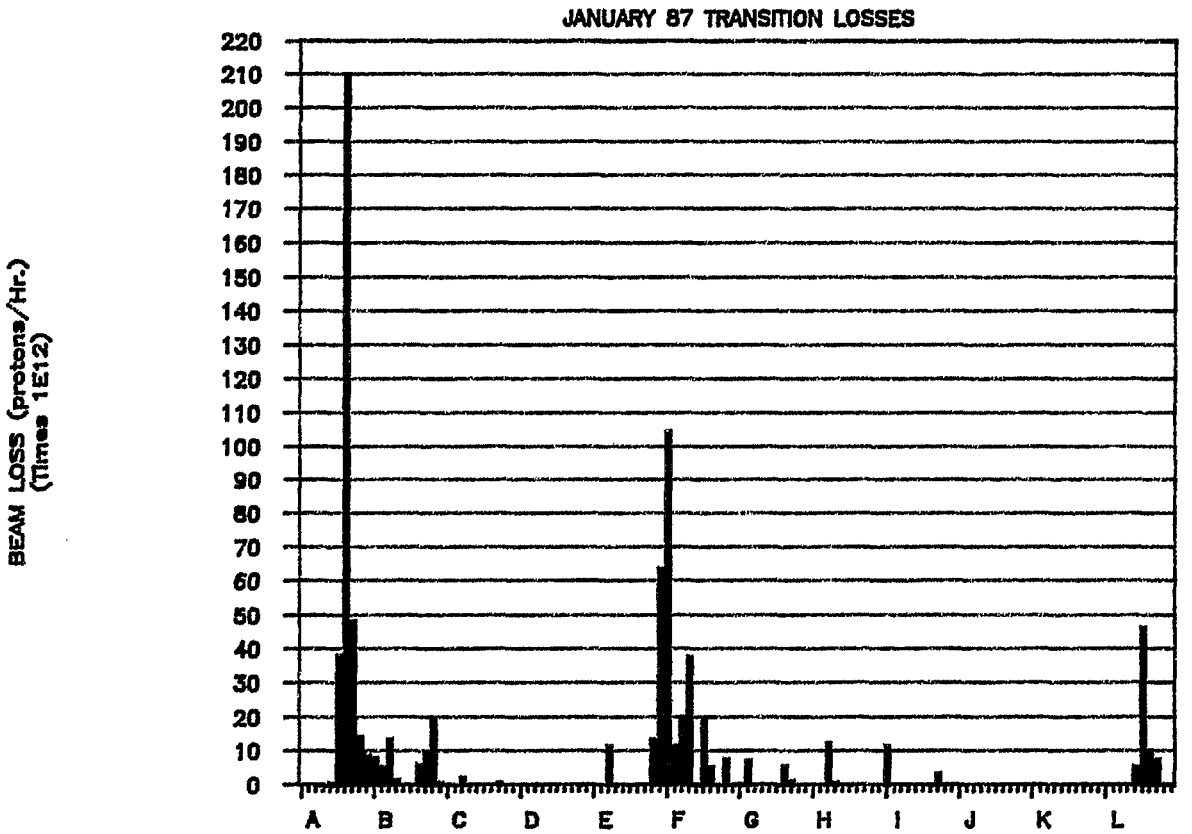

FIGURE 9: WT. AVG. LOSS DISTRIBUTIONS

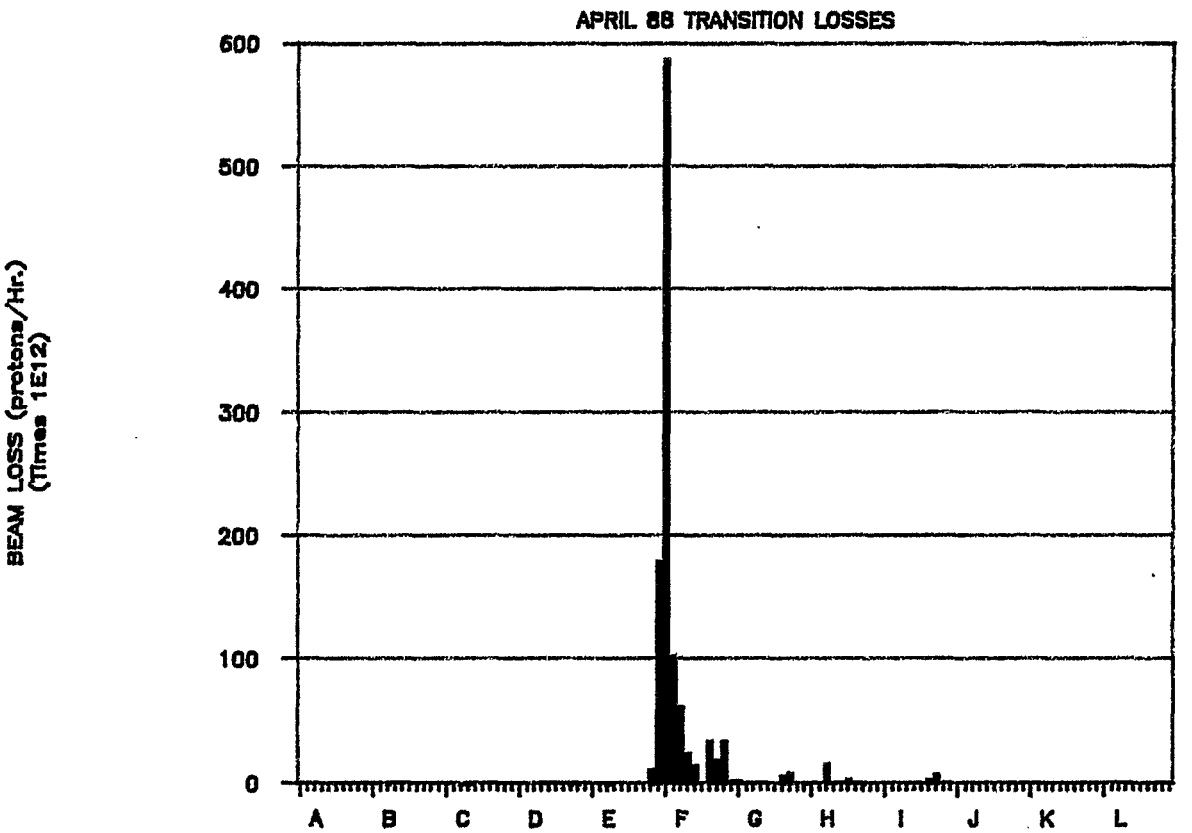

FIGURE 10: WT. AVE. LOSS DISTRIBUTIONS

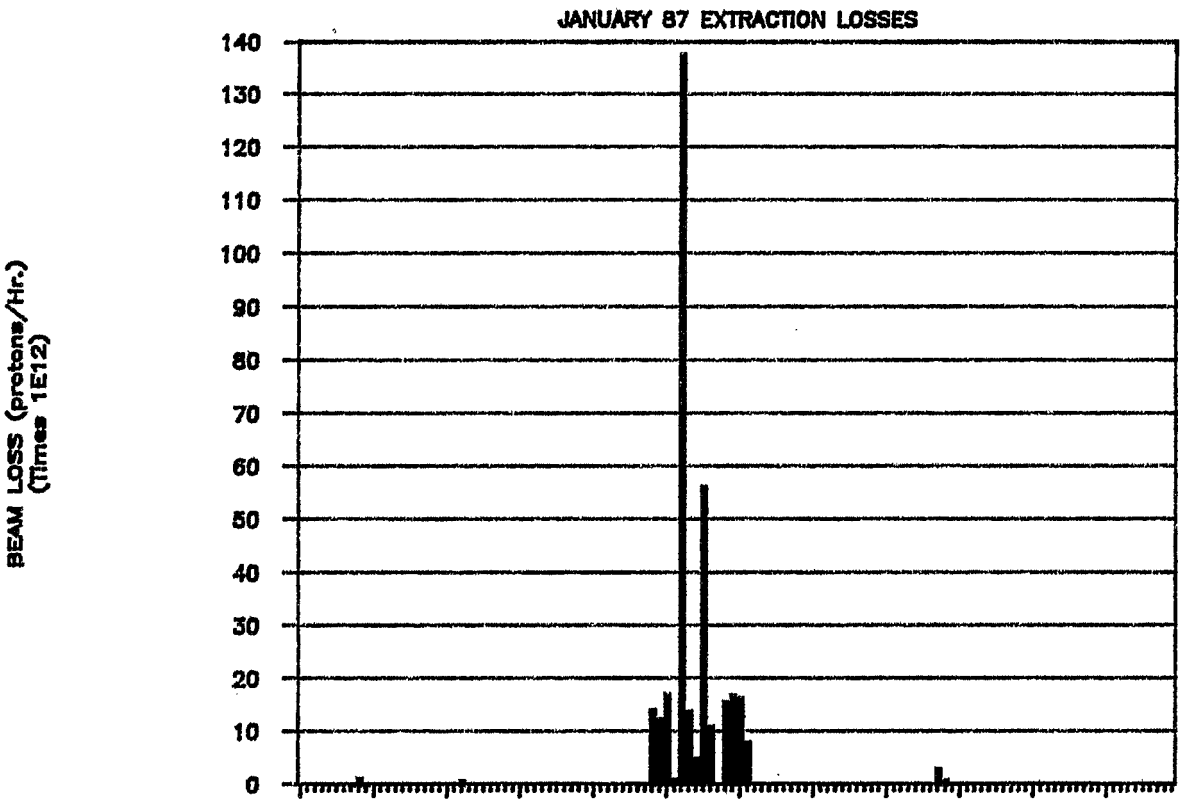

FIGURE 11: WT. AVG. LOSS DISTRIBUTIONS

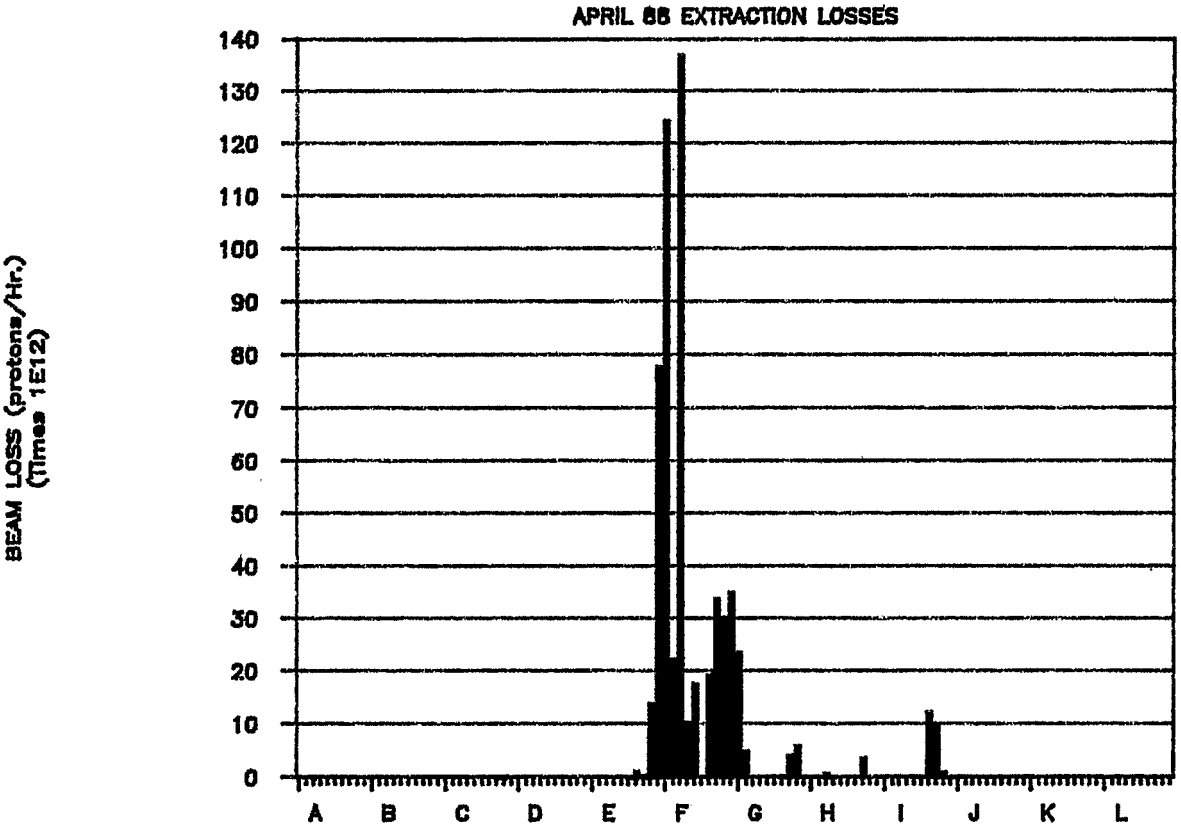

FIGURE 12: VALUES OF k/g vs POSITION

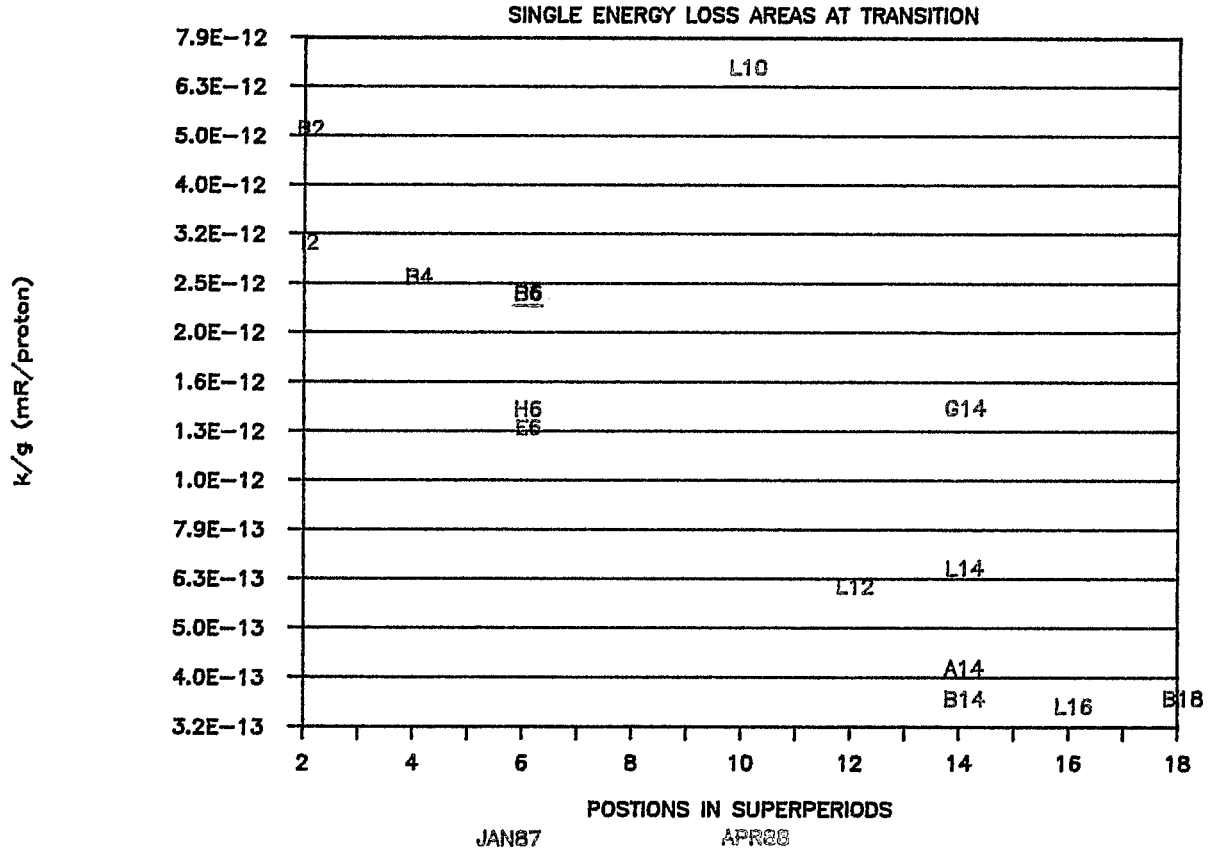

FIGURE 13: VALUES OF k/g vs POSITION

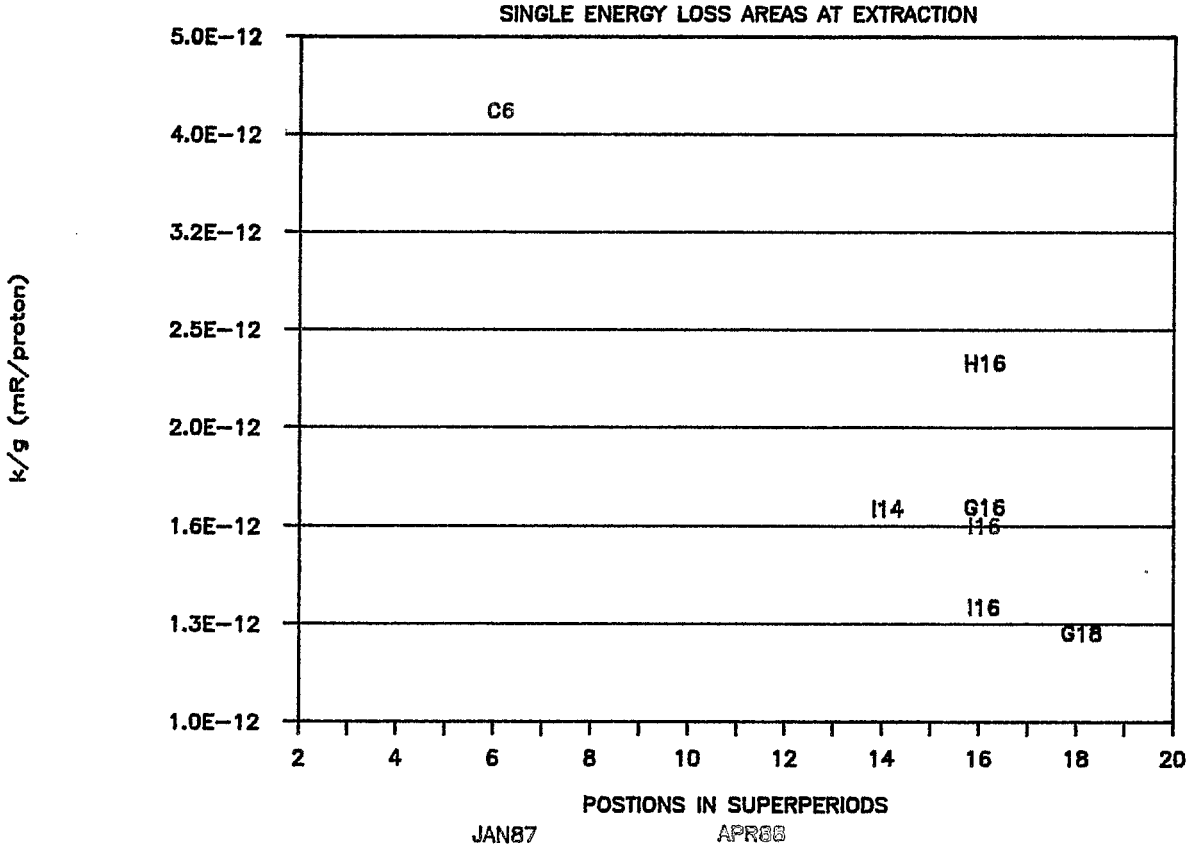

FIGURE 14: VALUES OF k/g vs POSITION

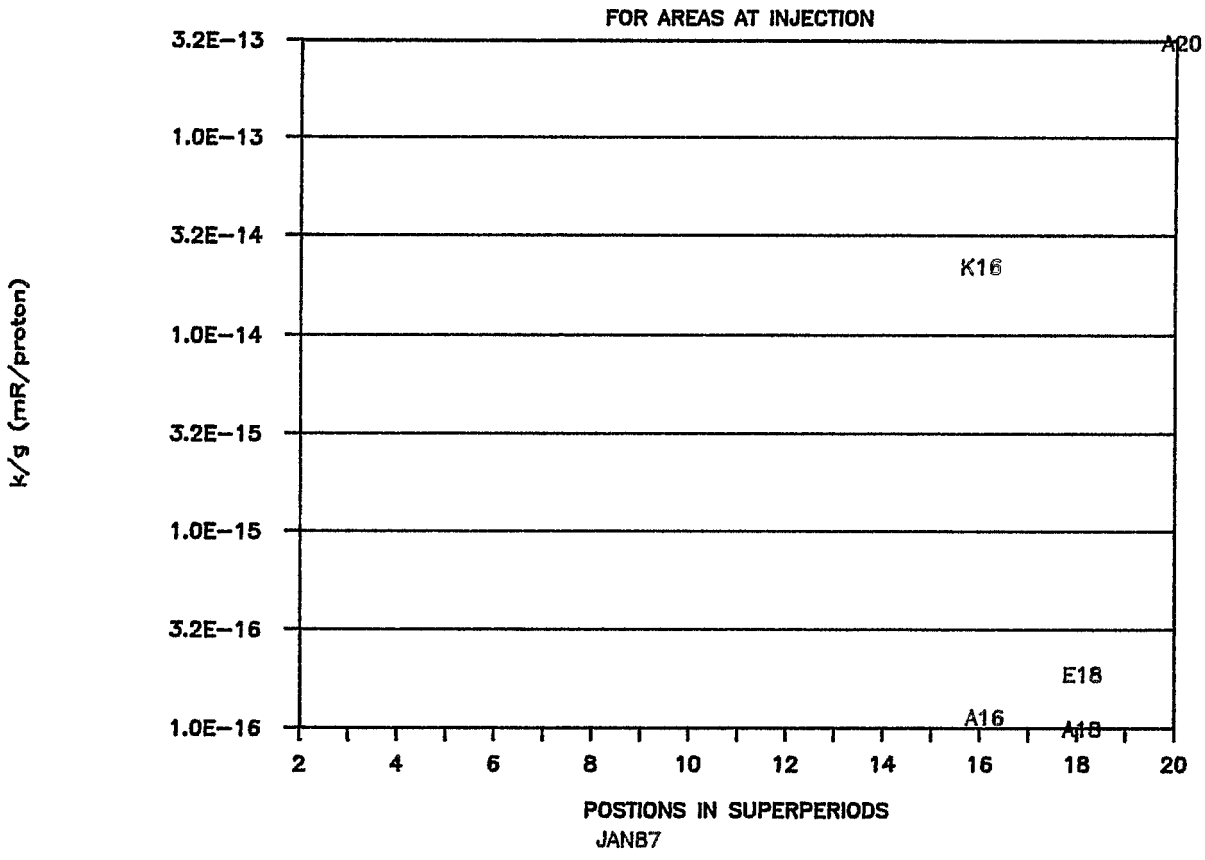

FIGURE 15: VALUES OF k/g vs POSITION

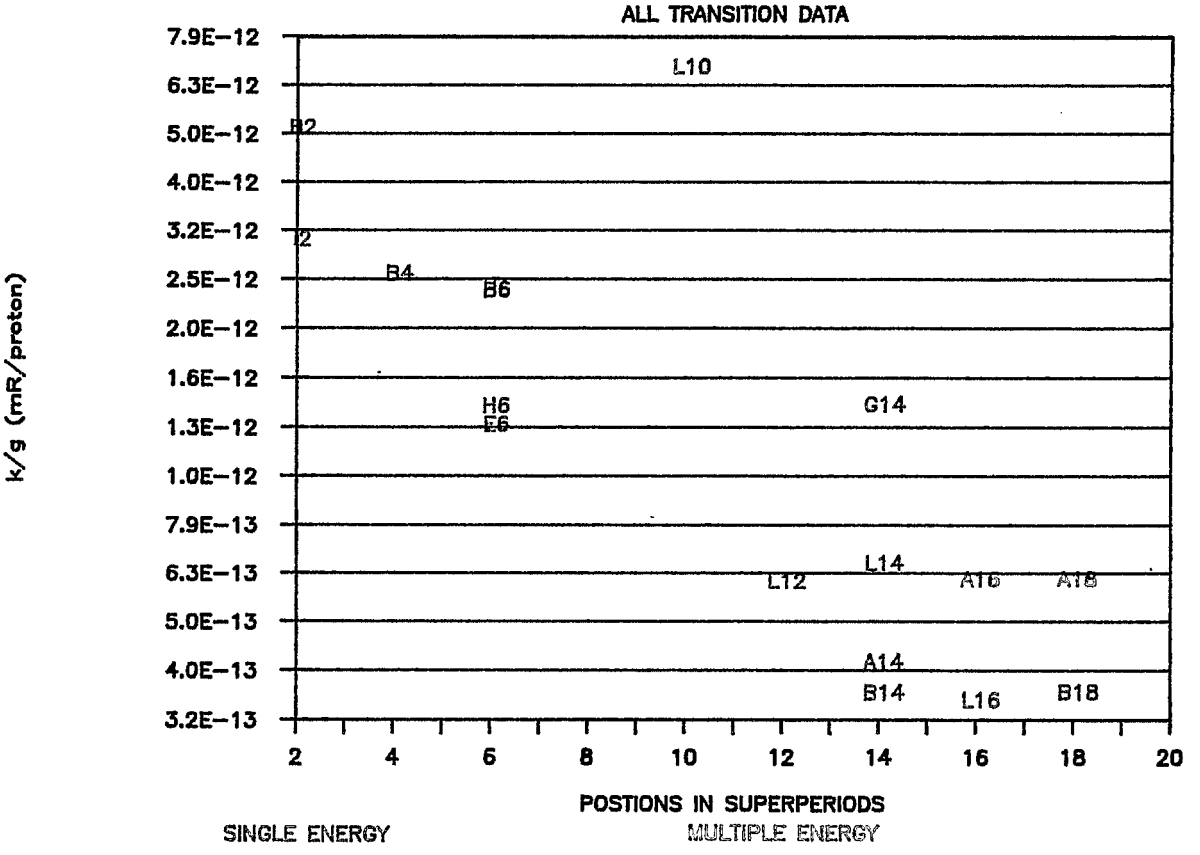

FIGURE 16: VALUES OF k/g vs POSITION

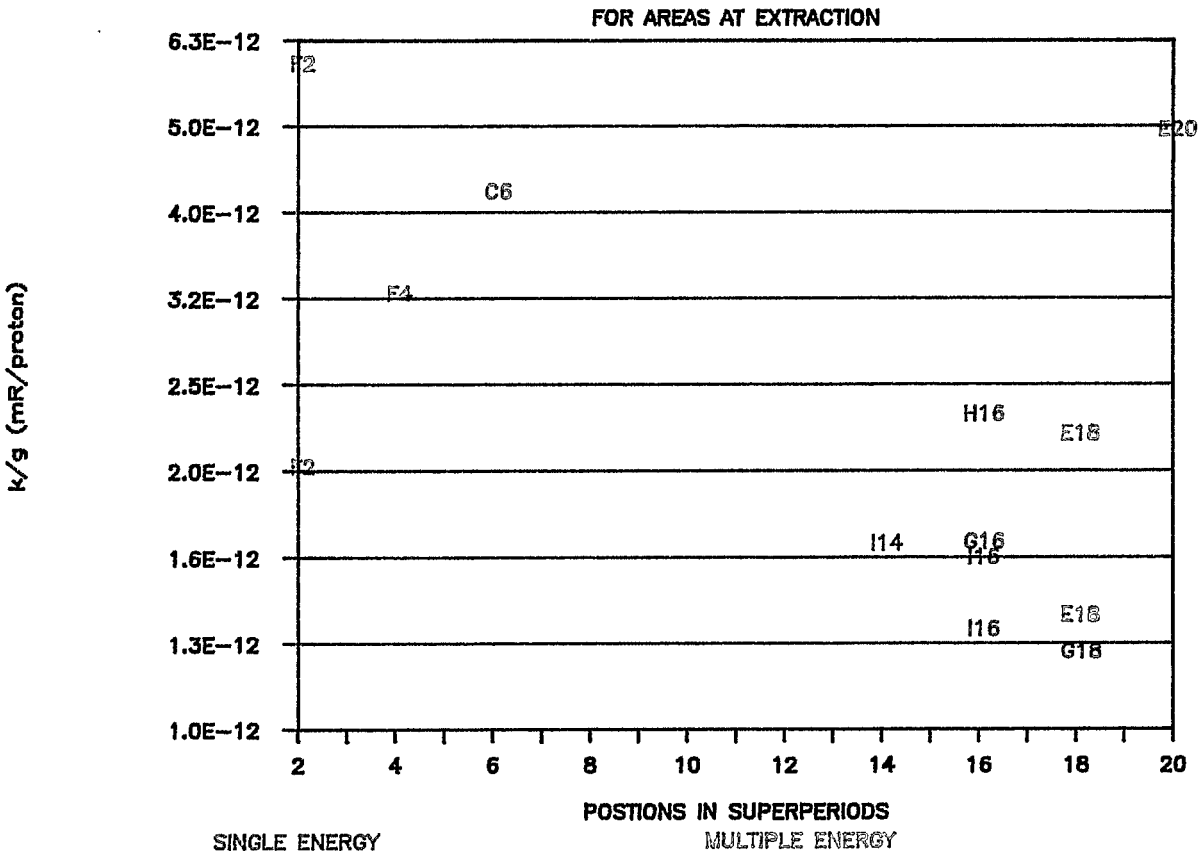

FIGURE 17: VALUES OF k/g vs POSITION

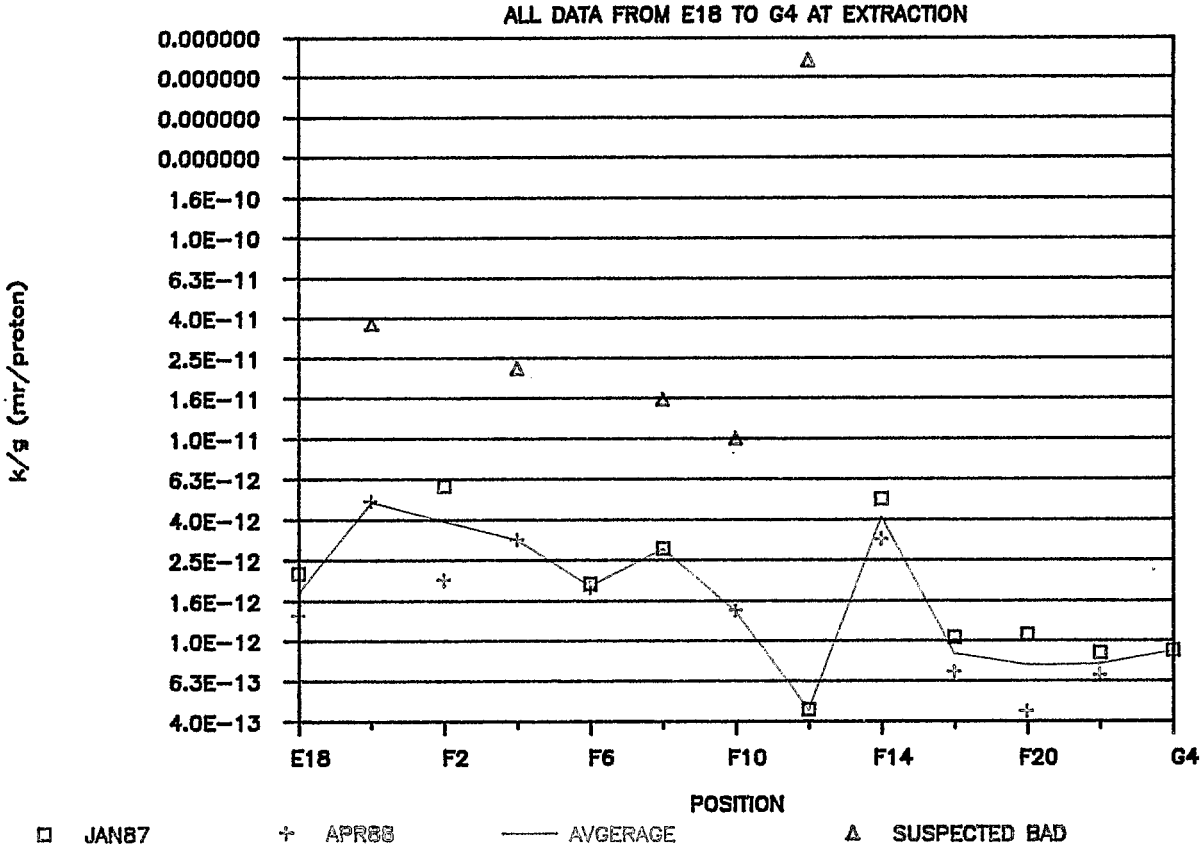

FIGURE 18: VALUES OF k vs BEAM ENERGY

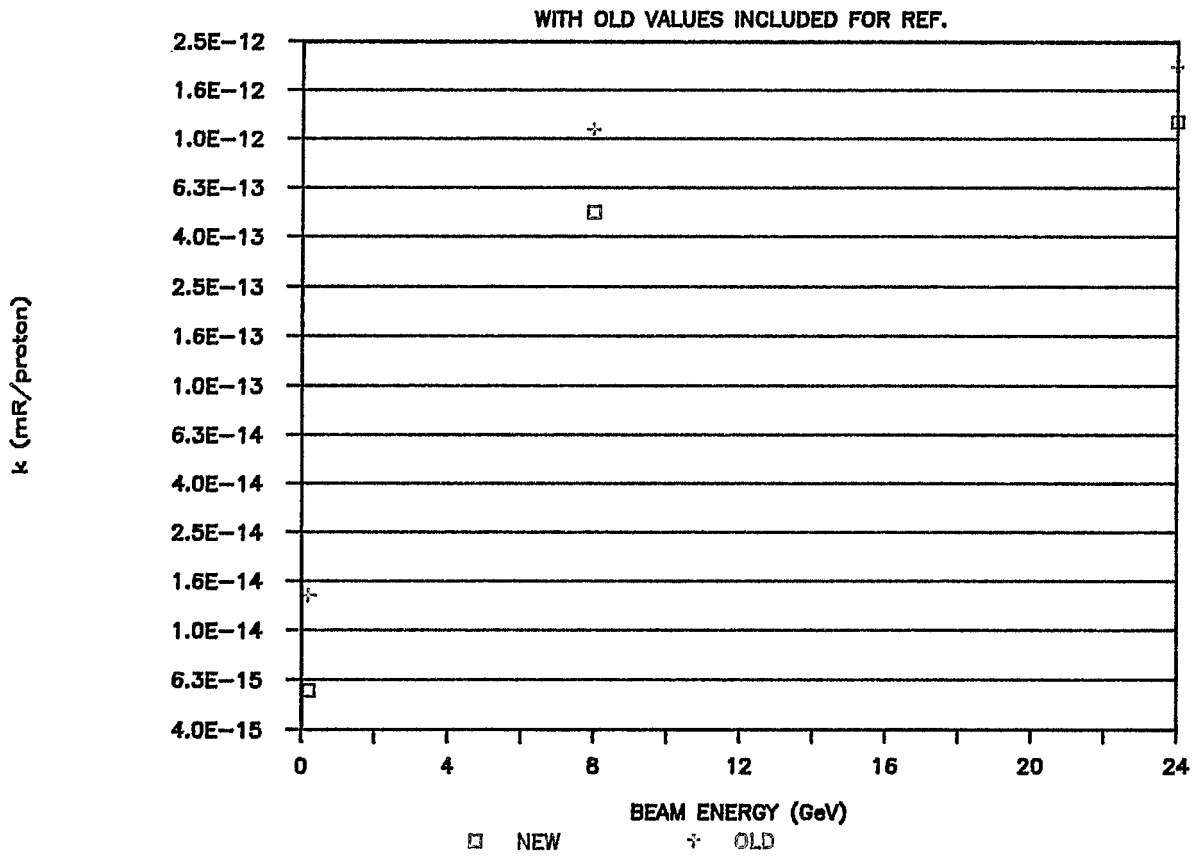

FIGURE A1: ISODOSE vs RADIAL POSITION

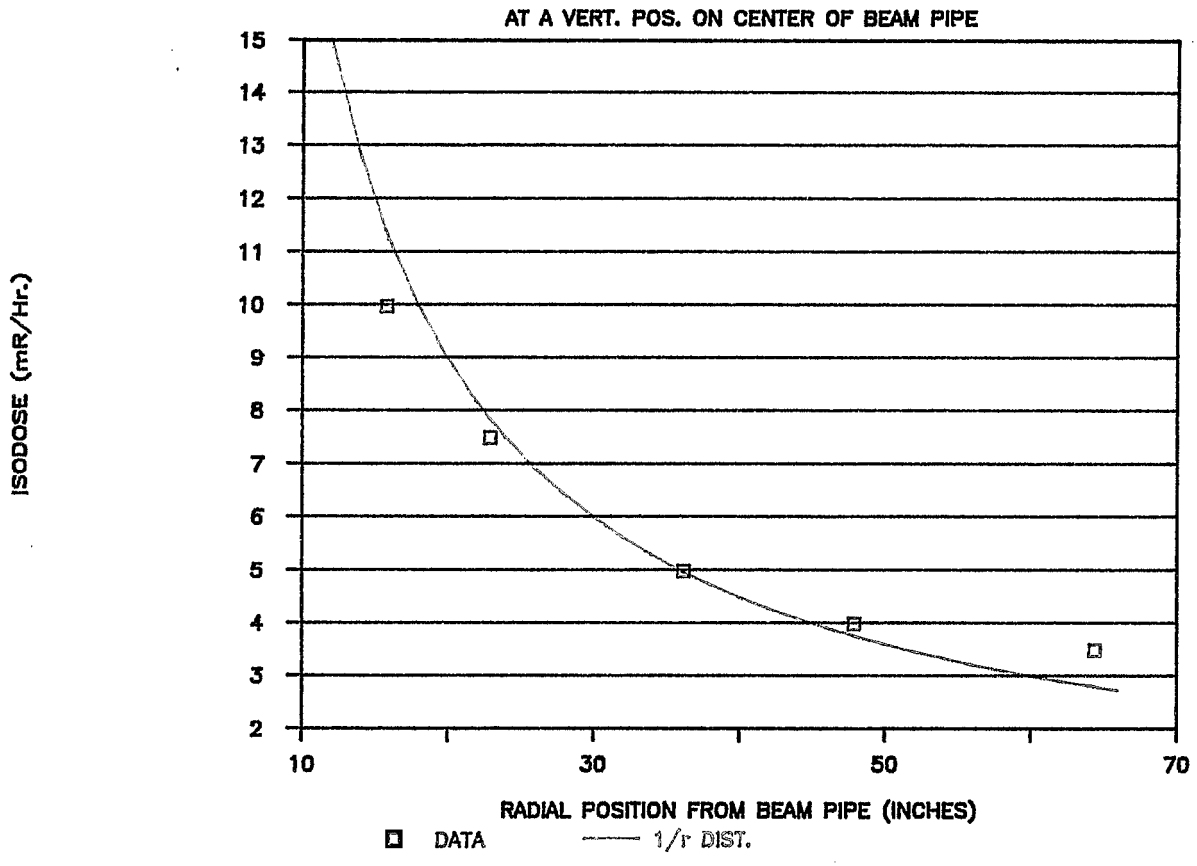

FIGURE A2: ISODOSE vs VERTICAL POSITION

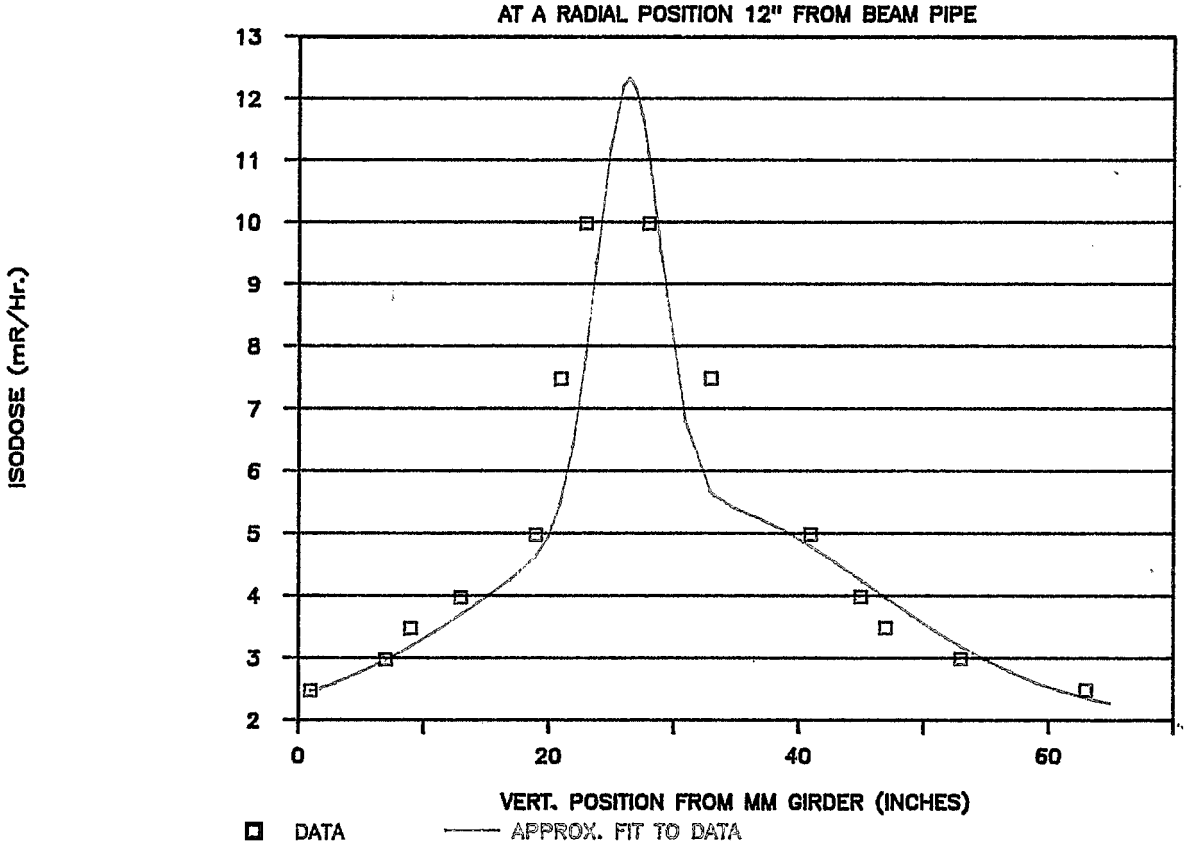

FIGURE A3: DISTRIBUTION OF ERRORS

FOR JANUARY ADDED ACTIVATIONS

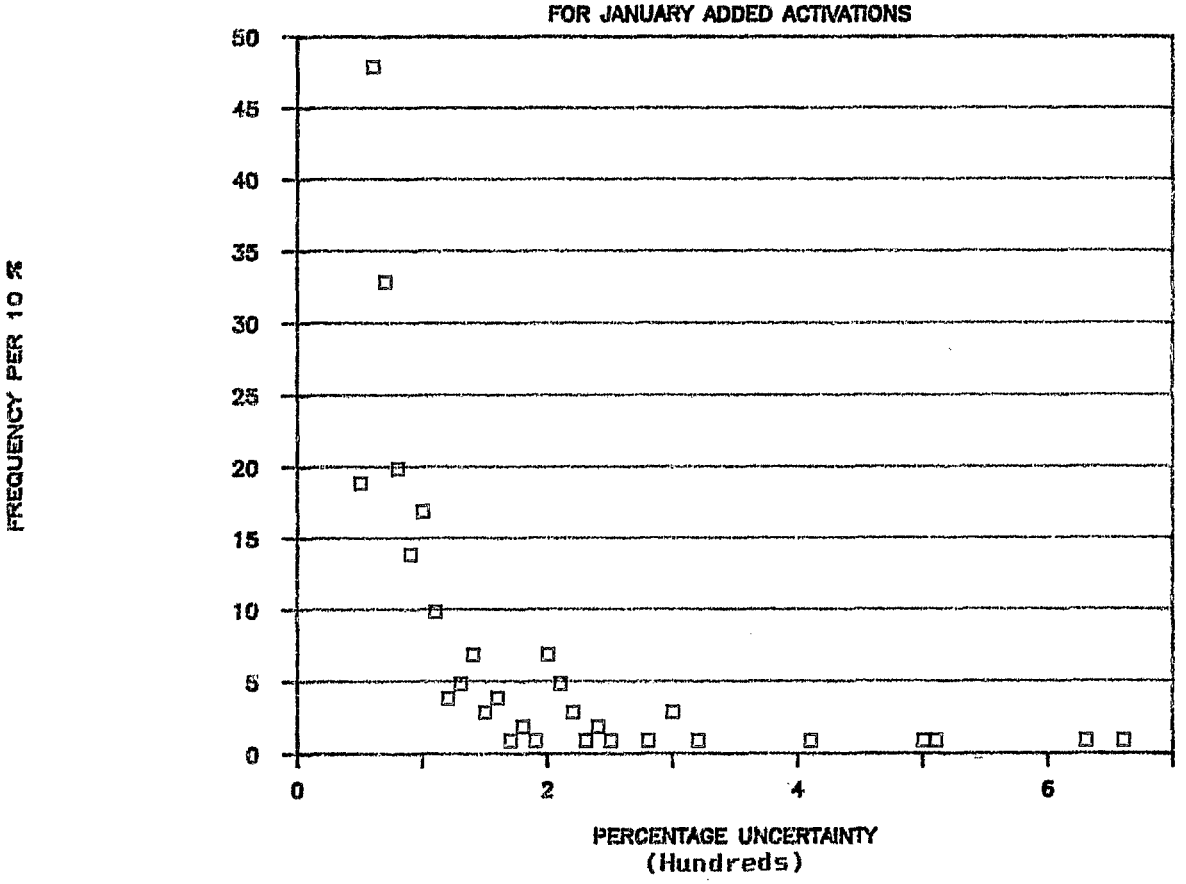

FIGURE A4: % UNCERTAINTY vs ACTIVATION

FOR JANUARY ADDED ACTIVATION DATA

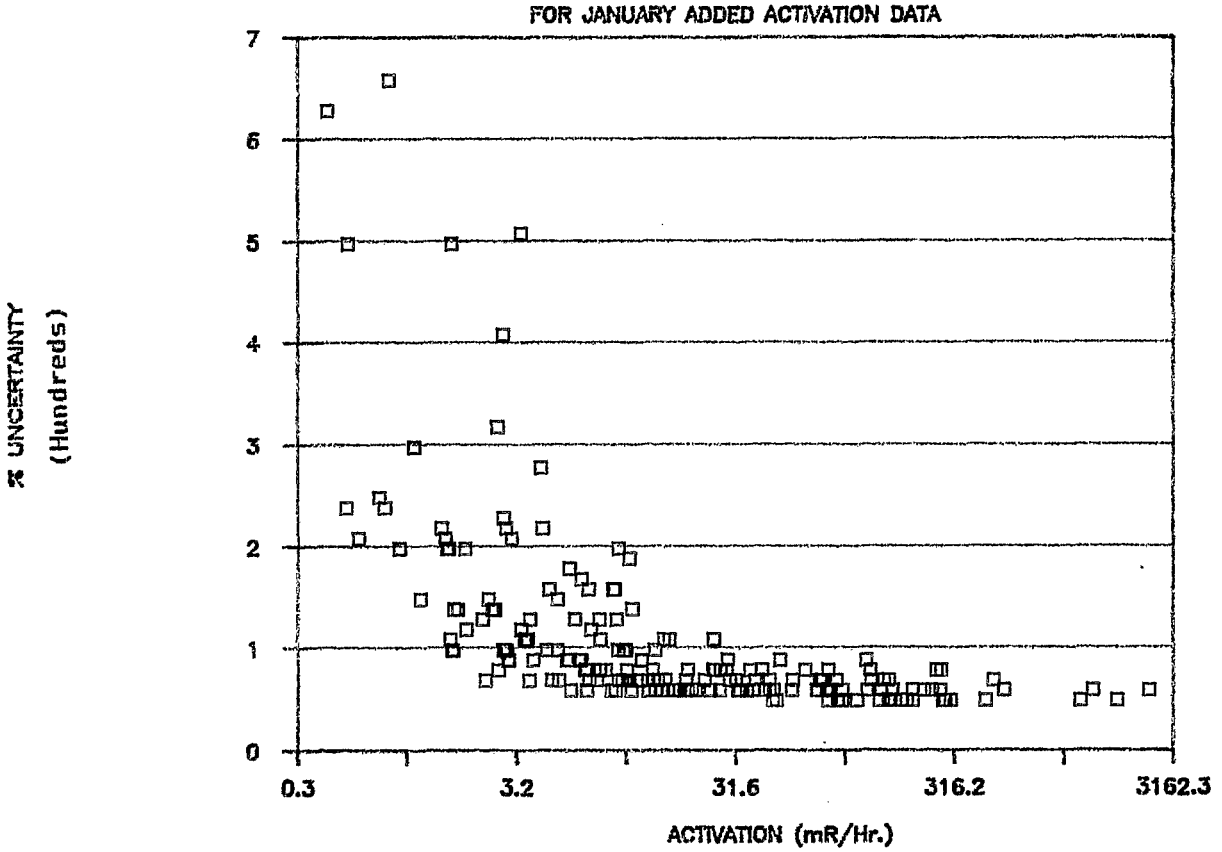

FIGURE A5: STANDARD DEVIATION vs LOSS

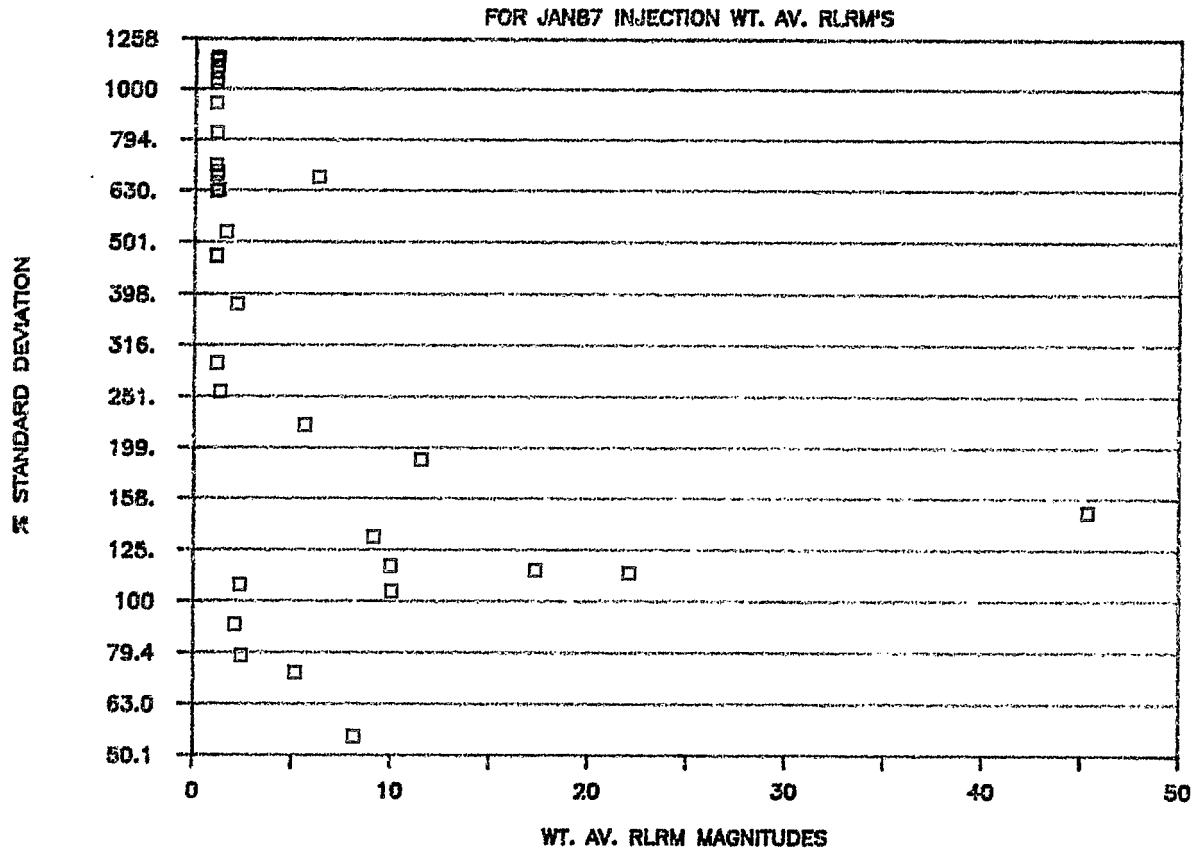

FIGURE A6: STANDARD DEVIATIONS vs LOSS

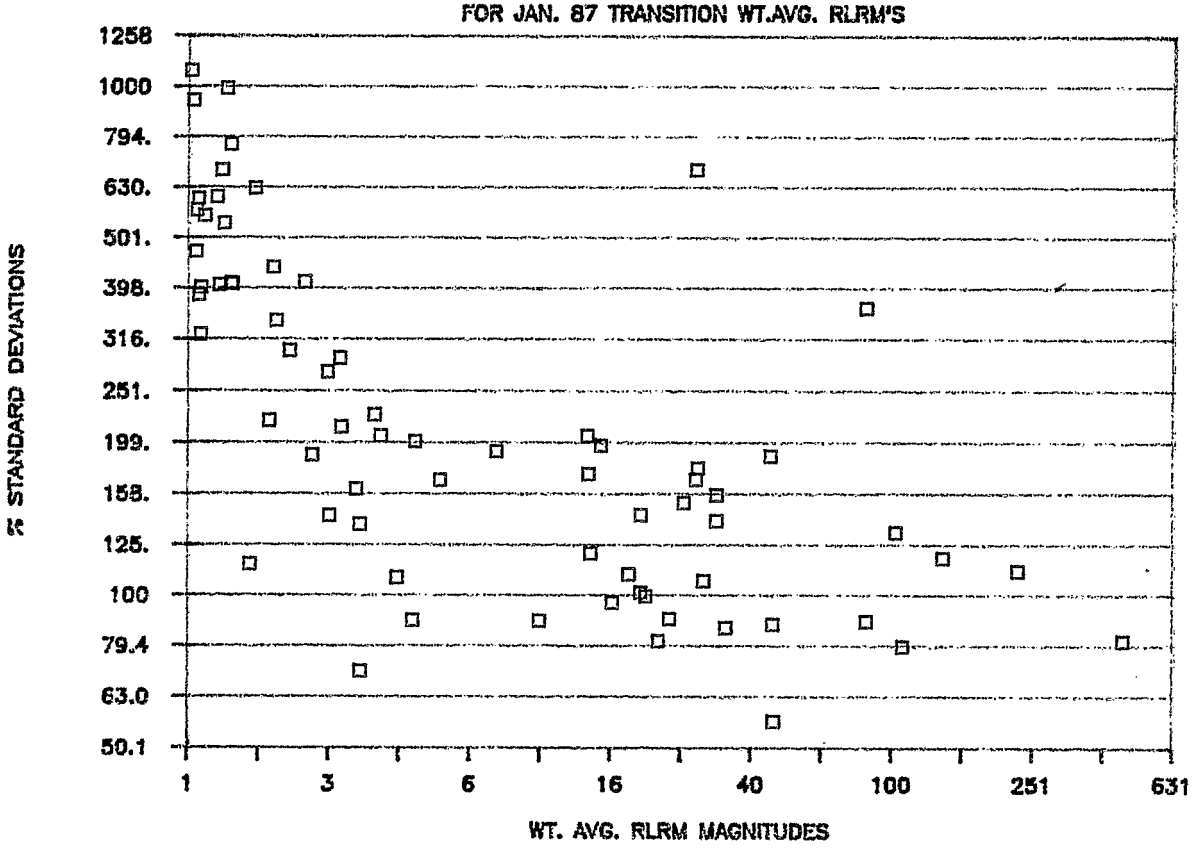

FIGURE A7: STANDARD DEVIATIONS vs LOSS

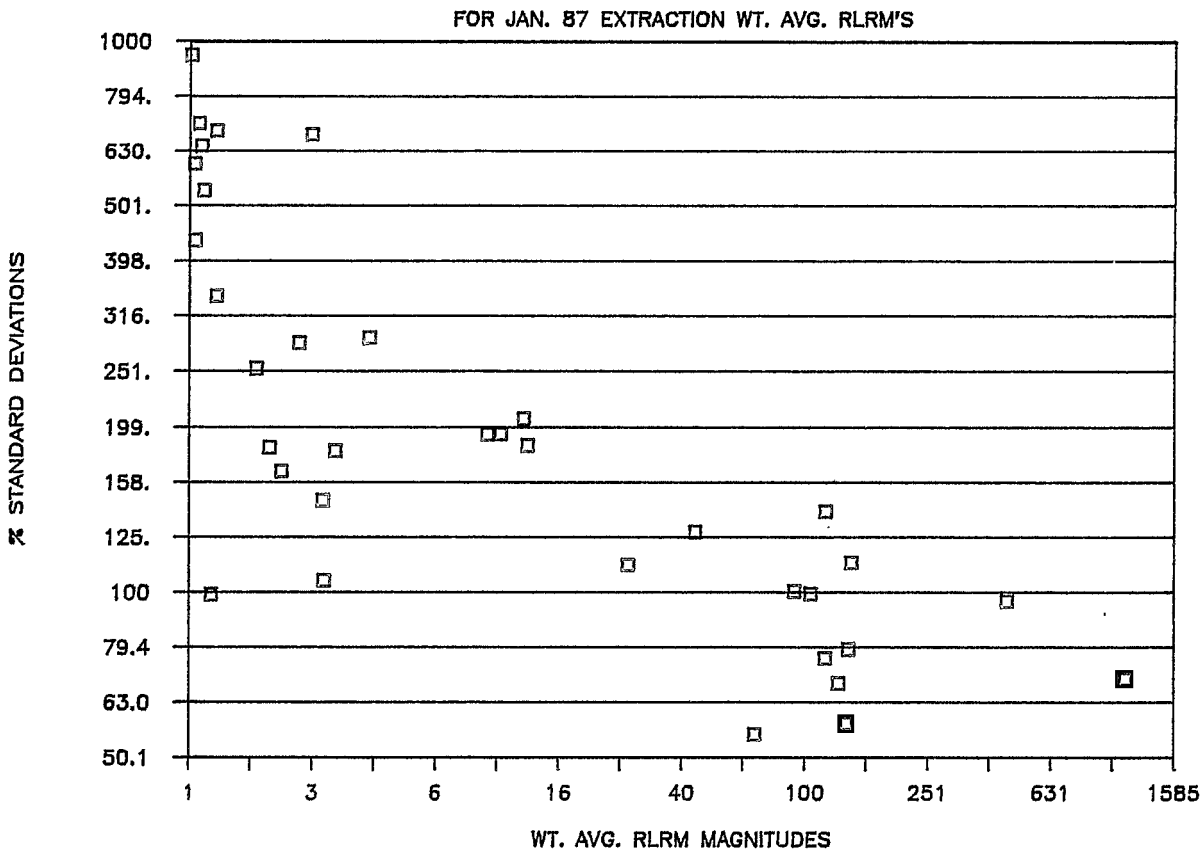

FIGURE A8: STANDARD DEVIATION vs LOSS